



Experimental study on multiple propagation characteristics of stress wave and surface displacement behavior in coal based on SHPB and DIC

Xiaoliang Li^{1,2} · Enlai Zhao^{1,2} · Zhentang Liu^{1,2} · Yubing Liu^{1,2} · Xiaojun Feng^{1,2} · Zhoujie Gu^{1,2}

Received: 28 April 2022 / Accepted: 23 May 2023 / Published online: 8 June 2023
© Springer-Verlag GmbH Germany, part of Springer Nature 2023

Abstract

Understanding the damage evolution behavior of coal under stress wave can provide a theoretical basis for preventing rock burst. In this work, the impact experiments of coal samples were carried out by split Hopkinson pressure bar (SHPB); the stress wave propagation characteristics were recorded by dynamic strain acquisition instrument; the evolution behaviors of coal samples' surface displacement were analyzed by digital image correlation (DIC); the correlation between stress wave and displacement were discussed based on the multi-fractal theory. The results proved the stress wave propagates in the non-linear attenuation mode of multiple incidences, reflection, and transmission. Among them, the attenuation velocity of the incident wave is the largest, followed by the reflected wave, and the transmitted wave is the smallest. The incident and reflected stress waves are mainly dominated by high amplitude signals, while the transmitted stress waves are mainly dominated by low amplitude signals. The horizontal displacement on the coal sample surface is changed in the form of variable velocity, acceleration, and direction during the process of the stress wave propagation. The impact velocity is favorably linked with the amplitudes and attenuation velocities of incident, reflected, and transmitted waves as well as the surface displacement, displacement velocity, and acceleration of coal samples. The multi-fractal characteristic parameters of stress wave and displacement show that the proportional relationship and difference between the large- and small-scale displacement are influenced by those between the high- and low-intensity signal of the stress wave, and the transmission wave can exert greater influence.

Keywords SHPB · DIC · Stress wave · Displacement · Multi-fractal characteristics

Xiaoliang Li is the first author.

✉ Enlai Zhao
zhel8215@163.com

Xiaoliang Li
tb19120010b2@cumt.edu.cn

Zhentang Liu
0973@cumt.edu.cn

Yubing Liu
liuyubing@cumt.edu.cn

Xiaojun Feng
xiaojun.feng@cumt.edu.cn

Zhoujie Gu
guzhoujie1996@163.com

Introduction

Rock burst, as a destructive mine earthquake induced by mining activities, seriously threatens the safe production of mines with its sudden, sharp, and violent damage characteristics, and has caused huge economic losses and casualties to coal mines in China (Wang et al. 2019; Vardar et al. 2022; Yang et al. 2022). The occurrence of rock burst can not only cause roadway damage and casualties, but also induce coal and gas outburst, gas explosion, roof accident, and other major underground malignant accidents (Zhao et al. 2018; Mondal and Roy 2019; Zhang et al. 2021; Liu et al. 2022b, 2023; Li et al. 2023; Yang et al. 2023). It seriously affects the safe and efficient mining of coal mines.

Numerous field studies have proved that the occurrence of rock burst can be significantly affected by various disturbance factors in coal mining (Gu et al. 2023; Tian et al. 2023), such as hard thick roof fracture (Wang et al. 2015), coal fracture in stress concentration area (Zhou et al. 2011), thrust fault slip

¹ Key Laboratory of Coal Mine Gas and Fire Prevention and Control of the Ministry of Education, China University of Mining and Technology, Xu Zhou, Jiangsu 221116, China

² School of Safety Engineering, China University of Mining and Technology, Xu Zhou, Jiangsu 221116, China

(Wang et al. 2017; Yang et al. 2019; Wang and Luan 2022), engineering blasting (Wu et al. 2019), and mining disturbance (Zhou et al. 2022). As a result, dynamic load would be generated and then propagate in the form of stress waves in coal and rock strata (Feng et al. 2016). When the stress wave propagates in the coal and rock stratum, it will refract, reflect and scatter, leading to a strong stress concentration around the free surface. When the dynamic stress is greater than the strength of the coal, the coal will be damaged, which will induce the rock burst (Feng et al. 2020b; Tan et al. 2021). So, it is necessary to study the propagation characteristics of stress waves and the damage evolution behavior of coal and rock under dynamic loading.

Hopkinson pressure bar is an important instrument for studying the dynamic behavior of coal and rock in the laboratory (Kai-Xin and Xu-Dong 2006; Li et al. 2008). Many scholars have used this equipment to study the propagation characteristics of stress waves and the mechanical behavior of coal and rock under dynamic loads. These studies mainly focus on the propagation and attenuation laws of stress waves (Ju et al. 2007; Xia et al. 2008; Han et al. 2022), the transfer model of stress waves (Li and Ma 2010; Ma et al. 2011), the influence of joint characteristics on transmission and reflection coefficients (Li et al. 2011a, b; Wu et al. 2014; Chai et al. 2016; Li et al. 2017b, 2019b), the relationship between the transmissive and reflective characteristics of stress waves and external load forms (Li et al. 2019a; Kong et al. 2021a, 2022), the strength of coal and rock (Huang et al. 2010; Li et al. 2016), the deformation of coal and rock (Tan et al. 2018), the energy evolution laws (Hong et al. 2009; Liu et al. 2015), the propagation forms of surface cracks in coal and rock (Chen et al. 2009; Dai et al. 2010), the dynamic constitutive model and equation of coal and rock (Ma et al. 2017; Kong et al. 2021b; Hou et al. 2023), and the fracture morphology (Zhang and Zhao. 2013; Li et al. 2021c). The results show that the stress waves propagate in coal and rock in the form of incidence, reflection, and transmission (Li et al. 2008). For a constant impact velocity, the amplitude of the reflected wave increases as the porosity of the sample increases, while the amplitude of the transmitted wave decreases (Ju et al. 2007). However, with the surface roughness of the sample joint increases, the transmitted wave amplitude gradually decreases, while the reflected wave amplitude gradually increases (Li et al. 2011a, 2017b, 2019b). The existence of static stress in rock has a significant impact on the stress waveform. When the static stress is constant, the stress waveform at different locations is approximately the same, while when the static stress changes, the stress waveform at the same location changes greatly (Cheng et al. 2019). In addition, the attenuation of incident, reflected, and transmitted waves is closely related to impact velocity, axial pressure, and confining pressure (Kong et al. 2020). When the dynamic load is constant, with the increase of axial pressure and confining pressure, the strength of coal and rock

first increases and then decreases (Liu et al. 2019; Hao et al. 2020). Under the same axial pressure and surrounding rock conditions, with the increase of impact velocity, the strength of coal and rock materials increases within a certain range (Yao et al. 2019). The dynamic tensile strength of coal and rock is smaller than its dynamic compressive strength (Zhao et al. 2016; Ai et al. 2019). Different anisotropy of coal and rock leads to different dynamic tensile strength of coal and rock (Zhao et al. 2014; Wang et al. 2017). With the increase of bedding angle, the dynamic tensile strength of coal and rock first decreases and then increases (Zhao et al. 2017). During the dynamic failure process of coal and rock, the incident energy is mainly consumed by reflected energy and transmitted energy, while less incident energy is consumed in the form of absorbed energy (Yan et al. 2021). The axial fracture of coal is directly caused by the incident compressive stress wave, while the lateral fracture is caused by the tensile stress wave reflected from the interface between the coal sample and the transmission rod (Feng et al. 2020a). The initiation of surface cracks in the sample occurs in the direction of the incident wave, and the propagation rate of the cracks along the X–Y direction increases with the increase of impact velocity (Ai et al. 2019, 2020). The strain in the horizontal direction of the sample is significantly greater than the strain in the vertical direction (Ai et al. 2019, 2020). The failure mode of rock materials under dynamic load is mainly transgranular fracture, supplemented by intergranular fracture (Li et al. 2021b).

With the development of computer technology and image processing technology, the combination of high-speed camera and digital correlation technology has become an important auxiliary means to study the fracture characteristics of the samples under dynamic load. Digital image correlation (DIC) is a non-contact, optical, non-destructive, and full field method, which can track the deformation and strain of the sample surface (Gao et al. 2015; Xing et al. 2020; Li et al. 2022b). Many scholars have studied the failure process of the material under the dynamic load by the DIC measurement technology, which drawn many valuable conclusions. Among them, Zhou et al. (2018) used the modified SHPB experimental system to carry out dynamic compression and shear load tests on granite, analyzed the evolution law of surface strain field by using DIC measurement technology, and proved the feasibility and accuracy of using DIC measurement technology to characterize the damage evolution behavior of materials. Li et al. (2020a) carried out dynamic load experiments on granite with holes and obtained the evolution law of the maximum principal strain and local strain of the granite surface in the whole field using the DIC measuring system. Yan et al. (2021) used an improved SHPB system combined with DIC testing technology to test multi-fracture rock samples under static and dynamic coupling compression, obtained the evolution law of the

surface displacement field of rock samples, and proposed a new crack classification direction based on the displacement trend line method. Yue et al. (2022) studied the dynamic fracture behavior of rock samples with sharp V-shaped notches using the digital image correlation (DIC) method. The displacement field of the sample surface was obtained, and the stress intensity factor, dynamic stress intensity factor at the crack tip, and crack growth rate were got from the displacement.

However, the above scholars' research on the mechanical behavior of samples subjected to stress waves remains within the first wave propagation, ignoring the impact of multiple propagation of stress waves on the mechanical behavior of specimens. In fact, after the completion of the first stress wave propagation, the stress wave does not immediately disappear, but attenuates in the form of multiple incidence, reflection, and transmission, still causing sustained damage to the sample. Under a fixed impact load, the sample may be damaged by multiple actions of stress waves. If the sample is not broken during the first wave propagation process, it may be broken during the subsequent stress wave propagation process (Lu et al. 2017). Compared to the first wave, the crack propagation degree of the sample under the subsequent stress wave is greater (Hao et al. 2020), and the splash degree of the fragments is also stronger (Lai et al. 2022). Therefore, it is of great significance to study the attenuation behavior of stress waves and their impact on the specimen after the propagation of the first wave.

Due to the stress waves propagate and attenuate in the form of multiple incidence, reflection, and transmission, their time series signal evolution behavior is relatively complex. The surface displacement of coal sample varies continuously with the multiple incidence, reflection, and transmission of stress waves. The velocity and acceleration of displacement are non-linear and complex. If a mathematical method can be used to simply and comprehensively describe the changing laws of stress wave and displacement, as well as the relationship between them, the evolution behavior of stress wave propagation and displacement can be more intuitively understood. As a classical method of data statistics, multi-fractal theory can extract targeted research elements from complex and variable information and can concisely and comprehensively reflect the essential characteristics of complex time series (Lyubushin et al. 2013, 2014). Many scholars used the multi-fractal theory to obtain the response signals in the process of coal and rock failure: potential signals (Niu et al. 2022), acoustic emission signals (Liu et al. 2022a), and electromagnetic radiation signals (Li et al. 2022a). The multi-fractal characteristic parameters are used to characterize the damage degree and failure types of coal and rock. Therefore, if the stress wave signal and the surface displacement have the characteristics of multi-fractal, the corresponding multi-fractal parameters can be used to

characterize the multiple propagation behaviors of the stress wave, the displacement evolution laws, and the correlation between them.

In this paper, the impact tests of coal samples were carried out by the split Hopkinson pressure bar (SHPB). The super dynamic strain acquisition instrument of the SHPB experimental system was used to collect the voltage signals throughout the stress wave attenuation and summarize the multiple propagation laws. A digital image correlation (DIC) measurement system was used to analyze the changes in horizontal displacement, displacement velocity, and displacement acceleration of coal surface points during the stress wave multiple propagations. The multi-fractal theory guided the analysis of distribution laws of high and low amplitude signals in the stress waves and the variation characteristics of large-scale and small-scale displacement of coal sample surface points. Finally, the correlation was analyzed using their multi-fractal characteristics. The study can provide theoretical support for monitoring, early warning, and preventing the rock burst.

Experiment and processes

Experimental samples

The coal samples used in this experiment were taken from the Jining coal mine in Shandong, China. According to the experimental requirements, the specimens were made into 70 mm × 70 mm square samples after drilling, cutting, and polishing. The end face of the sample was perpendicular to the axis, with a maximum deviation of no more than 0.25°, and the parallelism of both ends was controlled to ±0.02 mm. The basic physical and mechanical characteristic parameters of coal samples used in this experiment are shown in the Table 1.

After processing the coal sample, it is necessary to make speckles on the surface of the coal sample. The sample surface is sprayed with white paint with a thickness of 1 mm as the background color. After the white paint on the surface of the coal sample is dry, the sample surface is randomly sprayed with black scattered spots of different sizes by black paint.

Experimental instruments

The equipment used in this experiment is the SHPB experimental system (Fig. 1), which is composed of an incident rod, a transmission rod, an energy absorber, an axial compression loading system, a bullet launching system, a laser velocimeter, a dynamic strain acquisition instrument, a high-speed image acquisition system, four strain gauges, two Wheatstone bridges, and the connectors. Among

Table 1 Basic parameters of coal samples

Number	Density (g/cm ³)	<i>P</i> wave velocity(m/s)	Elastic modulus (GPa)	Poisson's ratio
1	1.33	1452	1.90	0.28
2	1.33	1425	1.89	0.28
3	1.32	1410	1.89	0.30
4	1.34	1472	1.91	0.29
5	1.34	1486	1.90	0.30
6	1.32	1494	1.91	0.29
7	1.33	1506	1.90	0.30
8	1.34	1478	1.88	0.30
9	1.32	1448	1.91	0.29
10	1.34	1436	1.88	0.28
11	1.33	1446	1.89	0.28
12	1.33	1428	1.88	0.28

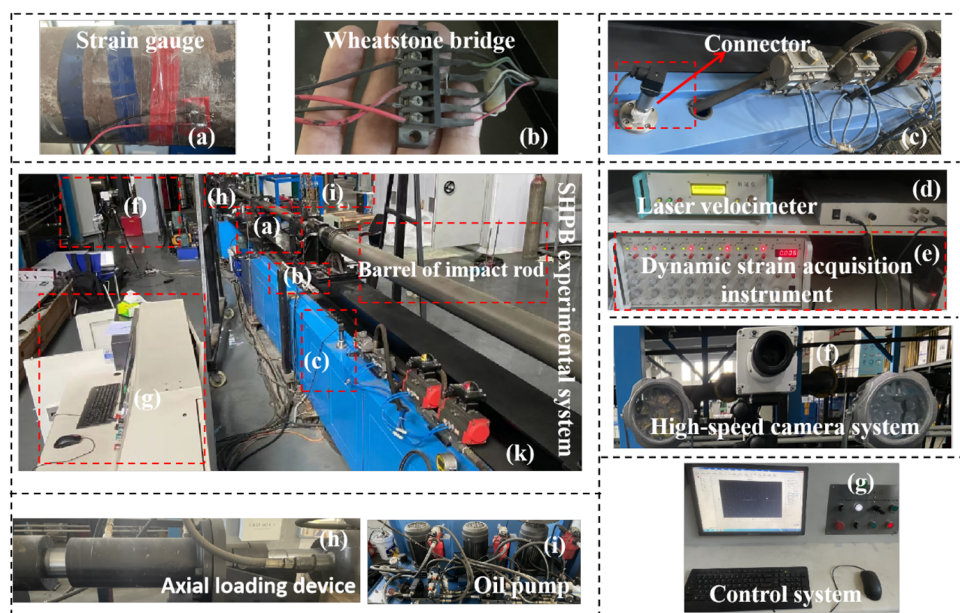
them, both the incident rod and the transmission rod are high-strength steel with a diameter of 100 mm, and their lengths are 5000 mm and 3000 mm, respectively. The elastic modulus was 210 GPa, and the longitudinal wave velocity was 5100 m/s. The overall view of the SHPB experimental system is shown in Fig. 1k, and the detailed views of each subsystem are shown in Fig. 1a to i. The strain gauges were attached at the distance of 2000 mm from the incident rod/transmission rod (near the side of the coal sample), and they were connected to the connector through a Wheatstone bridge. The connector and the dynamic strain gauge were connected through wires. The high-speed camera system consists of a high-speed camera and two lighting fixtures.

Among them, the high-speed camera is connected to the control system through wires. The axial pressure loading system consists of an axial pressure loading device and an oil pump.

The DIC test system consists of a high-speed system and Match ID-2D software, among which the high-speed camera used in this experiment is Phantom VEO710L. The minimum time interval between two exposures is 300 ns, and the sensitivity (ISO) is 32,000. The camera has a maximum shooting frequency of 1,000,000 fps/s and a maximum resolution of 1280 × 800. The shooting frequency in this experiment is 200,000 fps/s. That is, take a picture every 5 microseconds. The resolution at this shooting frequency (200,000 fps/s) is 128 × 128. The Match ID software can calculate the global and local displacement, displacement velocity, displacement acceleration, strain, and other parameters of the sample surface. The boundary compensation function in the software can ensure that the surface boundary of the sample is also effectively calculated. The performance analysis (PA) module in the software can realize the quantifiable DIC calculation results according to the optimization of the parameter settings, and the signal can be de-noised by setting the parameters such as subset, step size, strain filtering window, shape function, and interpolation algorithm.

Experimental process

The impact compression experiments with impact speeds of 1 m/s, 1.5 m/s, 2 m/s, and 2.5 m/s were carried out by the SHPB testing system. The data acquisition system, dynamic strain gauge, and strain gauge were used to collect the voltage signal of the stress wave attenuation process of the coal

Fig. 1 Experimental system

sample under the dynamic load. During the experiment, the strain gauge attached to the incident rod recorded the incident wave and reflected wave signals, while the strain gauge attached to the transmission rod recorded the transmission wave. The surface changes of coal samples were photographed by a high-speed camera, whose pictures were analyzed by Match ID-2D software in the DIC test system. First, start the axial loading device in the SHPB system, and the axial pressure of 1 MPa was used to fix the coal sample between the incident rod and the transmission rod; second, the air compressor in the SHPB experimental system was used to inject air pressure into the air chamber in the bullet triggering system in the SHPB; third, unlock the laser velocimeter, the dynamic strain acquisition instrument, and the data acquisition system; fourth, start the pre-trigger system in the SHPB system to check whether the laser velocimeter and high-speed camera worked normally; and finally, start the synchronous trigger system in SHPB system for experiment. Each experiment was conducted three times to avoid experimental errors. The relevant data of the experiment were sorted out for further analysis and discussion.

Experimental results and discussions

The propagation characteristics of stress waves

The propagation process of the dynamic load stress wave is shown in the Fig. 2.

According to the principle of SHPB experimental system, the incident wave is recorded by the strain gauge attached to the incident rod before it propagates to the A_1 end of the coal sample. When the incident wave propagates to the A_1 end of the coal sample, it will generate reflection and transmission to form reflection and transmission waves. The reflected wave propagates in the opposite direction to the incident wave and is recorded by the strain gauge attached to the incident rod. Because the amplitude of the incident wave in this experimental system is negative, the amplitude of the reflected wave is positive. The transmitted wave passes

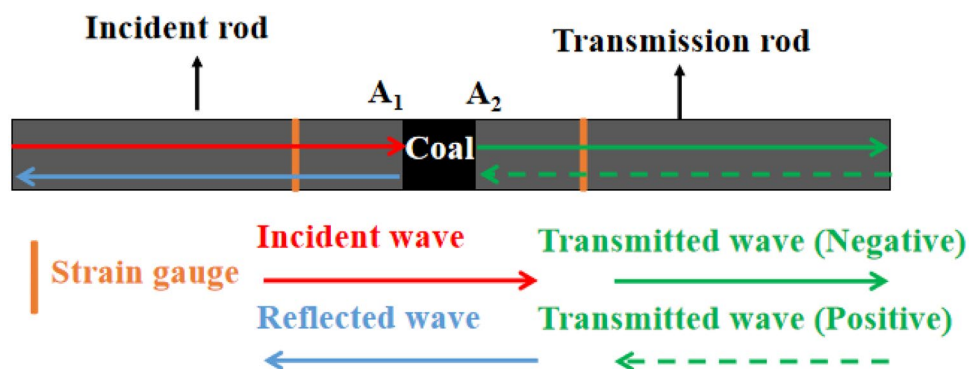
through the A_2 end of the coal sample and is recorded by the strain gauge attached to the transmission rod. At this experiment, the propagation direction of the transmitted wave is the same as the incident wave, but opposite to the reflected wave. Therefore, the amplitude of the transmitted wave is negative. When it propagates to the end of the transmission rod, the propagation direction of the transmission wave is reversed and recorded again by the strain gauge attached to the transmission rod. This time, the transmission wave was first recorded by the strain gauge attached to the transmission rod and then propagated to the A_2 end of the coal sample. So, the amplitude of the transmitted wave at this time is positive. Because positive transmission waves are generated by reversing the propagation direction of negative transmission waves, the positive transmission wave experiences a longer path and consumes more energy. Therefore, the absolute value of the amplitude of the positive transmission wave is smaller than that of the negative transmission wave. The stress waves propagate through coal in the form of multiple incidence, reflection, and transmission until they are depleted.

The propagation characteristics of the incident and reflected wave

Figure 3 shows the attenuation characteristics of the incident wave and reflected wave.

As shown in Fig. 3, the attenuation process of the incident wave and reflected wave is all non-linear. The amplitude of the end wave of the incident (reflected) is about 18 to 21% of its first wave. At different impact velocities, the attenuation modes of the incident and reflected waves are almost the same, but there are significant differences in amplitude. With the impact velocity increases, both the amplitude of the first and the end of the incident and reflected waves increase. When the impact velocity is 1 m/s, the amplitude of the first wave (end wave) of the incident wave and the reflected wave is -0.112 V (-0.022 V) and 0.106 V (0.020 V), respectively. When the impact velocity increases to 2.5 m/s, the amplitude of the first wave (the end wave) of the incident

Fig. 2 Propagation process of stress wave



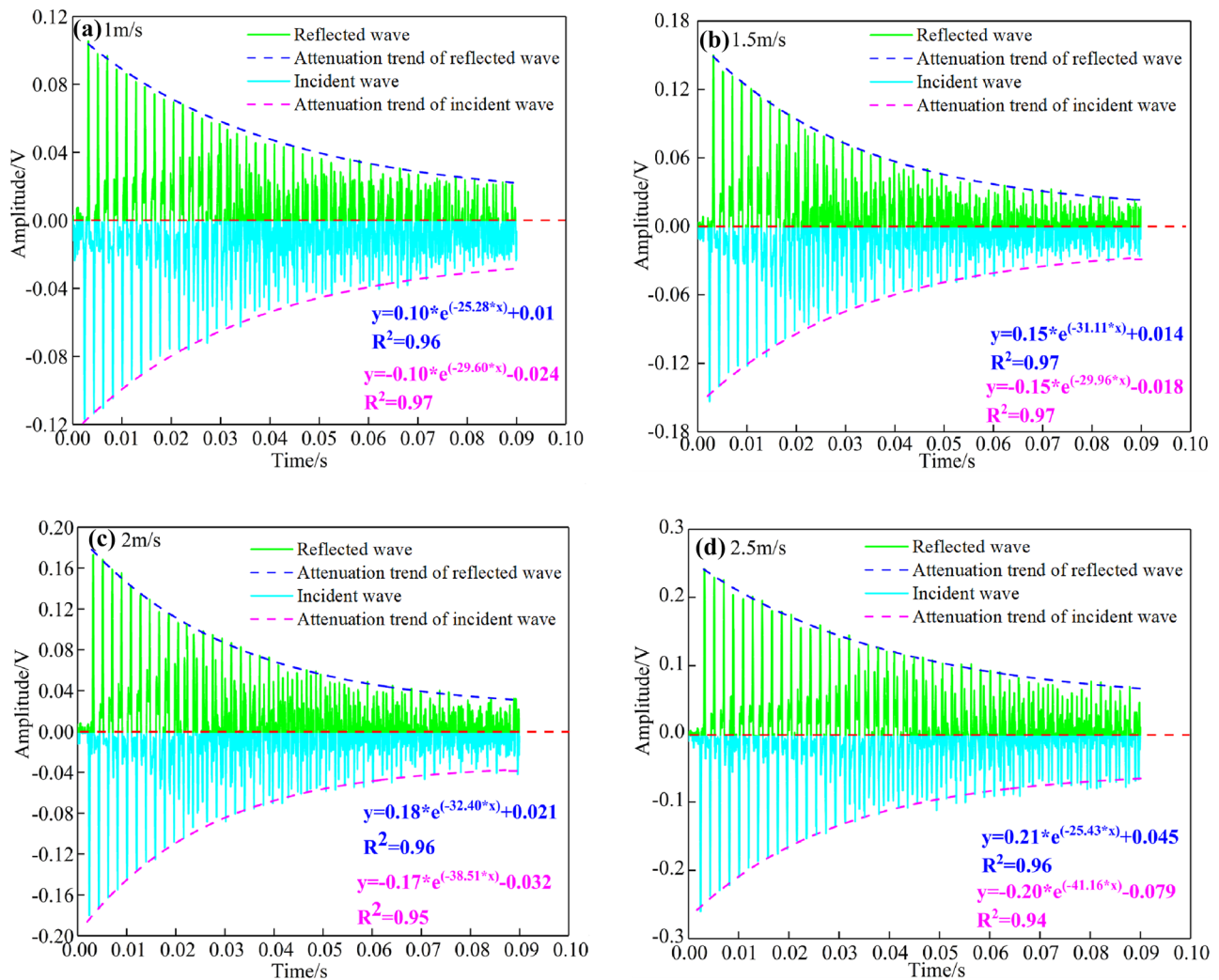


Fig. 3 The attenuation process of incident and reflected waves (**a**: 1m/s, **b**: 1.5m/s, **c**: 2m/s, **d**: 2.5m/s)

wave and the reflected wave is -0.261 V (-0.052 V) and 0.242 V (0.043 V).

The propagation characteristics of the transmitted wave

The attenuation characteristics of the transmitted wave are shown in Fig. 4.

As shown in Fig. 4, the attenuation mode of transmitted wave is the same as that of incident and reflected waves, but its amplitude is much smaller than that of incident and reflected waves. In addition, transmitted waves have two forms, positive negative transmission and positive transmission. When the transmitted wave first passes through the A_1 end of the coal sample and is recorded by the strain gauge attached to the transmission rod, the obtained transmission wave is the negative transmission wave (Fig. 2). The propagation direction of the negative transmitted wave is the same as that of the incident wave, but opposite to that

of the reflected wave. When the negative transmission wave propagates to the end of the transmission rod, its propagation direction is reversed. At this time, the transmitted wave first passes through the strain gauge attached to the transmission rod and then propagates to the A_1 end of the coal sample (Fig. 2). This type of transmitted wave is called the positive transmitted wave, and the propagation direction is the same as that of the reflected wave, but opposite to that of the incident wave. Compared to negative transmitted waves, the positive transmitted has a longer propagation path and consumes more energy. Therefore, the absolute value of the positive transmitted wave amplitude is less than that of the negative transmitted waves. With increased impact velocity, the first wave amplitudes of positive and negative transmitted waves continued to grow. When the impact velocity is 1 m/s, the maximum amplitudes of positive and negative transmitted waves are 0.0129 V and -0.0165 V, respectively. When the impact velocity increases to 2.5 m/s, the maximum

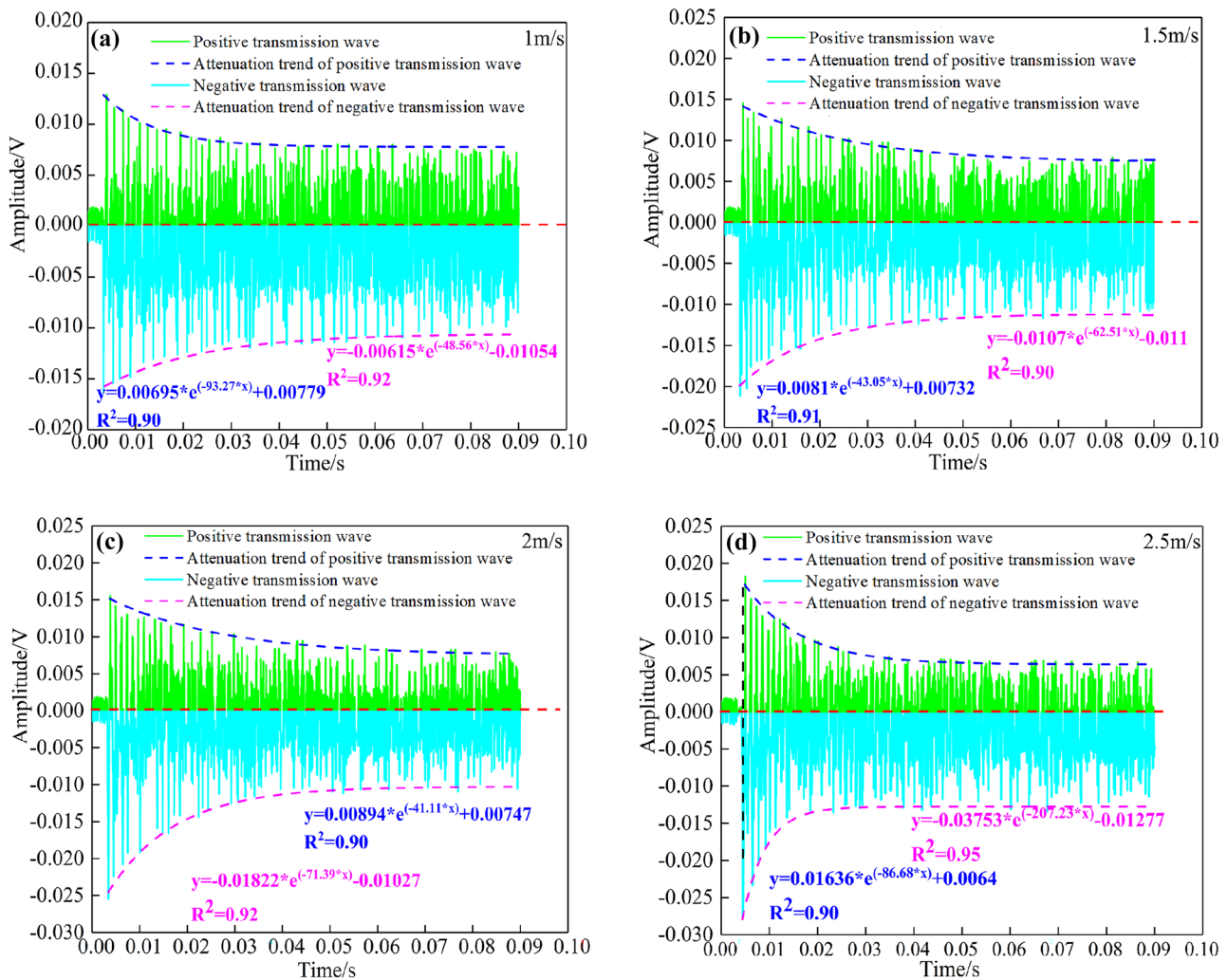


Fig. 4 The attenuation characteristics of the transmitted wave (a: 1m/s, b: 1.5m/s, c: 2m/s, d: 2.5m/s)

amplitudes of positive and negative transmitted waves are 0.0182 V and -0.0285 V, respectively. Therefore, the absolute value of the amplitude of the transmitted wave is positively correlated with the impact velocity.

The propagation velocity of the stress wave

In order to quantitatively characterize the evolution process of the stress wave attenuation velocity under different impact velocities, first, non-linear fitting is performed on the amplitude of the stress wave to obtain the attenuation trend line of the amplitude of the stress wave (Figs. 3 and 4). According to the fitting results, the fitting degree of the stress wave amplitude attenuation trend line exceeds 0.9, indicating a good fitting degree (Figs. 3 and 4). Then, the stress wave attenuation velocity trend line is obtained by solving the slope of the stress wave attenuation trend line (Figs. 5 and 6).

With the time increases, the attenuation velocities of the incident, reflected, and transmitted waves are not fixed, but decrease non-linearly; that is, the amplitudes of the incident, reflected, and transmitted waves are attenuated in the form of variable deceleration (Figs. 5 and 6). At the same impact velocity, the attenuation velocity of the incident wave is the largest, followed by the attenuation velocity of the reflected wave, and the attenuation velocity of the transmitted wave is the smallest. Taking the impact velocity of 1 m/s as an example, the attenuation velocities of the first incident wave, the reflected wave, the positive transmitted wave, and the negative transmitted wave are 2.81 V/s, 2.11 V/s, 0.25 V/s, and 0.47 V/s, respectively. It is worth noting that although the transmission wave has the smallest attenuation velocity, it takes the shortest time to reach a stable velocity. With the impact velocity increases, the attenuation velocities of the incident wave, reflected wave, positive transmitted wave, and negative transmitted wave all increase. When the impact

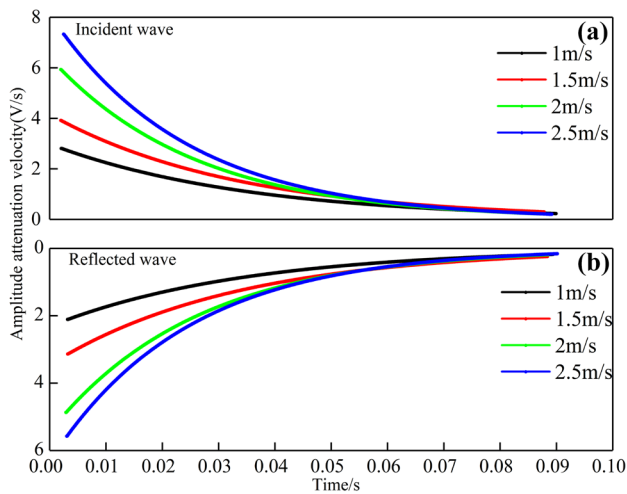


Fig. 5 Attenuation velocity of incident and reflected waves (a: Incident wave, b: Reflect wave)

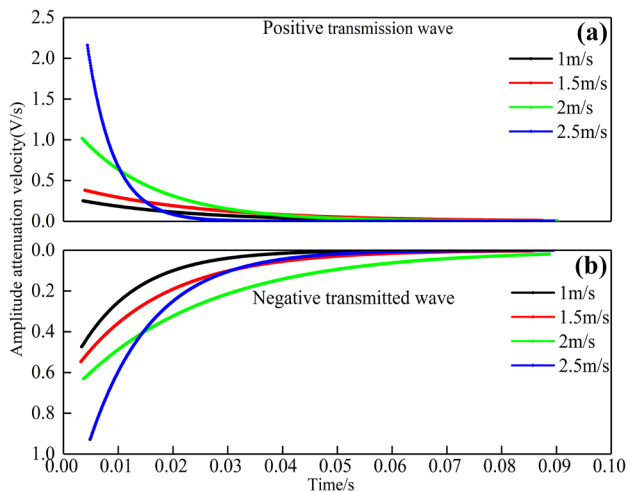


Fig. 6 Attenuation velocity of transmitted waves (a: Positive transmission wave, b: Negative transmission wave)

velocity is 2.5 m/s, the attenuation velocities of the first incident wave, reflected wave, forward transmitted, and negative transmitted wave are 7.31 V/s, 5.57 V/s, 2.16 V/s, and 0.93 V/s, respectively. Compared to the impact velocity of 1 m/s, it is increased by 2.60, 2.64, 8.64, and 1.98 times, respectively. So, not only the absolute values of the amplitude of incident, reflected, and transmitted waves are positively correlated with the impact velocity, but also their attenuation velocity is positively correlated with the impact velocity.

Displacement characteristics

During the stress wave attenuation, the incident, reflected, and transmitted waves continued to pass through the coal.

The stress wave always affected the coal, and its horizontal surface displacement was in dynamic changed (Fakhimi et al. 2018; Cong et al. 2021). So, the five points a, b, c, d, and e were selected on the coal surface (Fig. 7). The coordinates of points a, b, c, d and e are (10, 35), (22.5, 35), (35, 35), (47.5, 35), and (60, 35), respectively (Fig. 7). The changes of displacement at a, b, c, d, and e in the horizontal direction during the dynamic load stress wave were analyzed by the DIC measurement system.

The basic principle of the DIC method was to match the geometric points on the digital speckle image under different states of the object surface and track the movement of the points to obtain the deformation information of the object surface (Xing et al. 2020). The speckle on the coal surface was sprayed randomly, and the small area around each point on the speckle image was called sub-areas. The sub-areas centered on a certain point in the speckle field were used as the carrier of the displacement of the point (Golewski. 2021), which could be obtained by searching and analyzing the movement and change of the sub-area (Jobin et al. 2021; Yu et al. 2021). As shown in Fig. 5, the reference area S_1 centered on the feature point $P_1(x_1, y_1)$ is a sub-area with a size of 128×128 pixels. After the face moved, the sub-area S_1 moved to the position of the sub-area S_2 so that the deformed position $P_2(x_2, y_2)$ of the feature point P_1 was obtained. Thus, the displacement of the P_1 point was obtained. The evolution characteristics of the displacement field of the coal sample surface in the process of dynamic stress wave propagation were shown in Fig. 8 and Fig. 9).

As shown in the Fig. 8, the surface displacement of the coal sample increases with time during the first wave propagation ($t = 0 - 1.20$ ms), and the displacement direction is negative at this period. The coal sample surface experiences its maximum horizontal displacement following the first stress wave propagation, which is around seven times more than the maximum displacement experienced during the first wave. The displacement direction of the coal sample

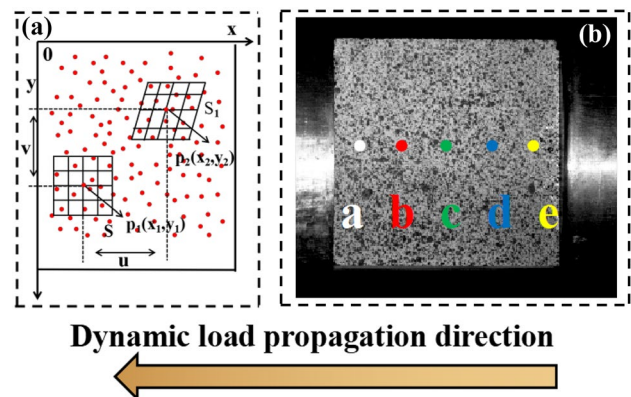


Fig. 7 DIC measurement principle (a: Calculation Principles, b: Coal sample testing)

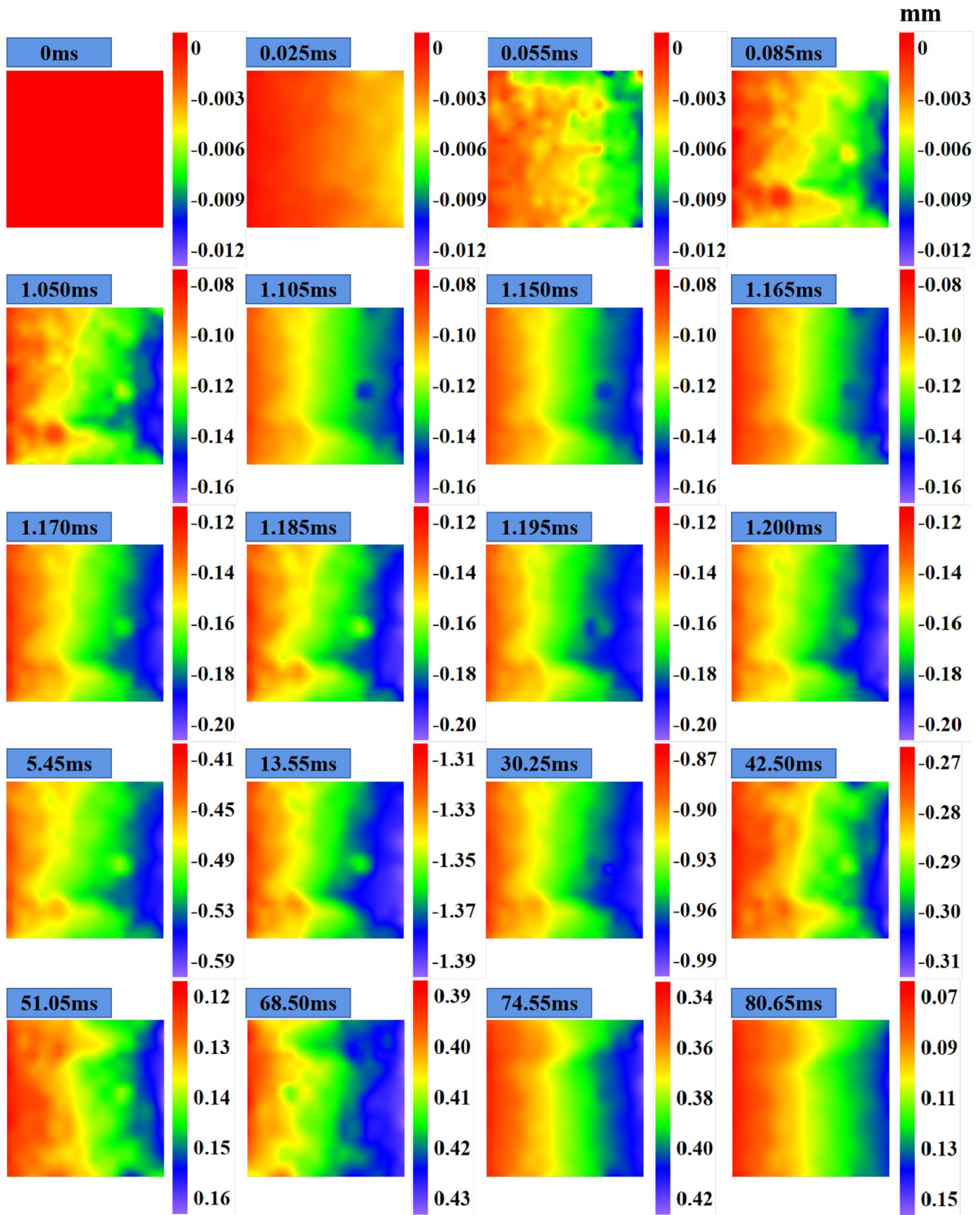


Fig. 8 Evolution process of surface displacement of coal samples (2.5 m/s)

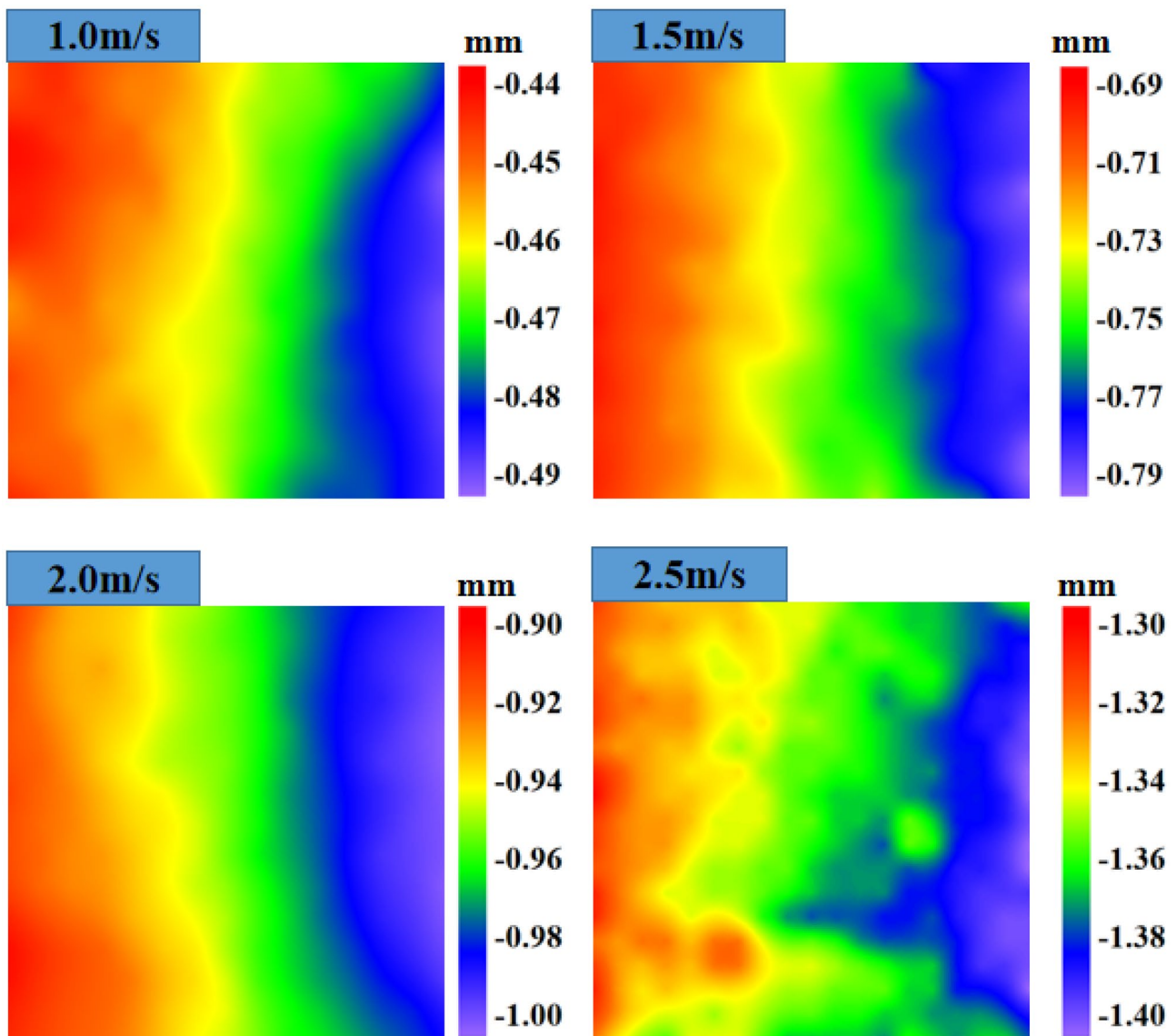


Fig. 9 Maximum surface displacement of coal samples (different impact velocity)

surface was changed between 51.05 seconds and 80.65 seconds. The maximum positive displacement was attained at 68.50 ms in time. The displacement tends to decrease in the positive direction after reaching its maximum positive value. Also, the coal sample's surface displacement shows a distribution pattern that is "small on the left and high on the right," which denotes that the displacement is larger close to the dynamic load source and smaller farther away from the dynamic load source. The greatest horizontal displacement of the coal sample surface rises along with the impact velocity. When the impact velocity is 1 m/s, the coal sample surface experiences the largest horizontal displacement of -0.49 mm, and when the impact velocity is 2.5 m/s, an increase of 2.98 times, the displacement increases to -1.40 mm. Although the maximum amount of horizontal

displacement on the surface of coal samples varies depending on the impact velocity (Fig. 9), the pattern of horizontal displacement distribution on the surface of the coal sample is almost the same under different impact velocities. The side closer to the dynamic load source (right) has greater displacement, and the side farther away from the dynamic load source (left) has smaller displacement.

According to the principle of DIC testing, the displacement change on the surface of the coal sample is caused by the movement of many points on its surface. The displacement changes of coal samples' surface points under different impact velocities are shown in the Fig. 10.

As shown in the Fig. 10, the value and direction of point displacement on the coal surface change in the form of oscillation in dynamic load stress wave attenuation. The

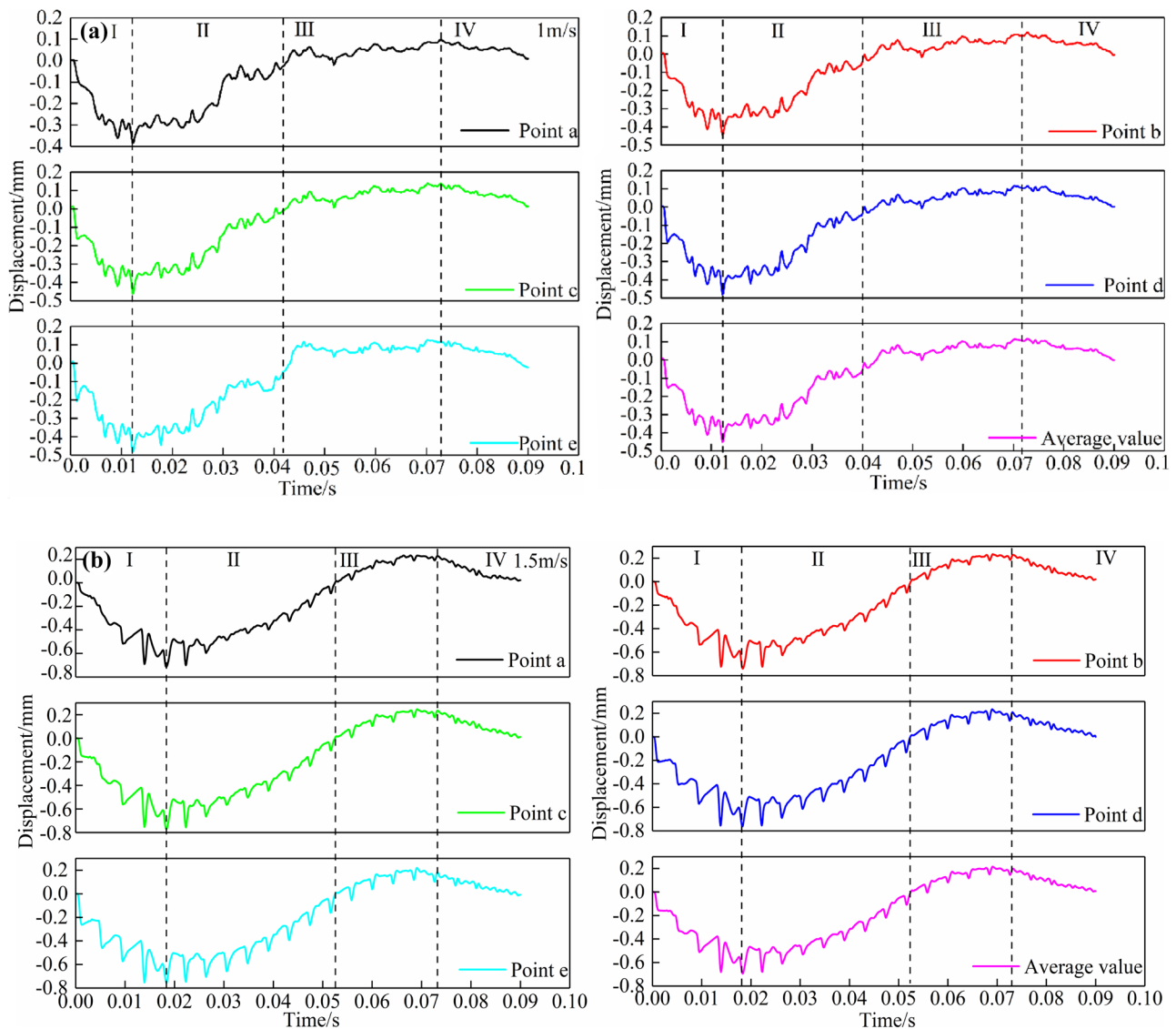


Fig. 10 Displacement of coal sample surface points (a:1m/s, b: 1.5m/s, c: 2m/s, d: 2.5m/s)

oscillation process included negative oscillation increasing period, negative oscillation decreasing period, positive oscillation increasing period, and positive oscillation decreasing period. The horizontal displacement of coal surface points has the same displacement degree in the negative oscillation increase period and the negative displacement decrease period. The displacement degree of the two was the largest in the four stages, but the negative oscillation increase period consumed a shorter time, showing that the displacement rate was the fastest during the increase period of negative displacement oscillation. When the displacement direction is negative, its moving direction is the same as the propagation direction of incident wave, but opposite to the propagation direction of reflected wave. At this time, the surface displacement of coal sample is mainly controlled

by the compression of stress wave. When the displacement direction is positive, its moving direction is the same as the propagation direction of reflected wave, but opposite to the propagation direction of incident wave. At this time, the surface displacement of coal sample is mainly controlled by the tension of stress wave. The displacement direction of coal sample surface is dominated by the compression and tension of dynamic load stress wave.

It is worth noting that when the first stress wave propagation ends, the displacement of the coal sample surface does not reach the maximum value, and the maximum horizontal displacement of the coal sample surface appears after the first stress wave propagation. At the same time, the direction of the maximum displacement during the stress wave propagation is the same as that during the first

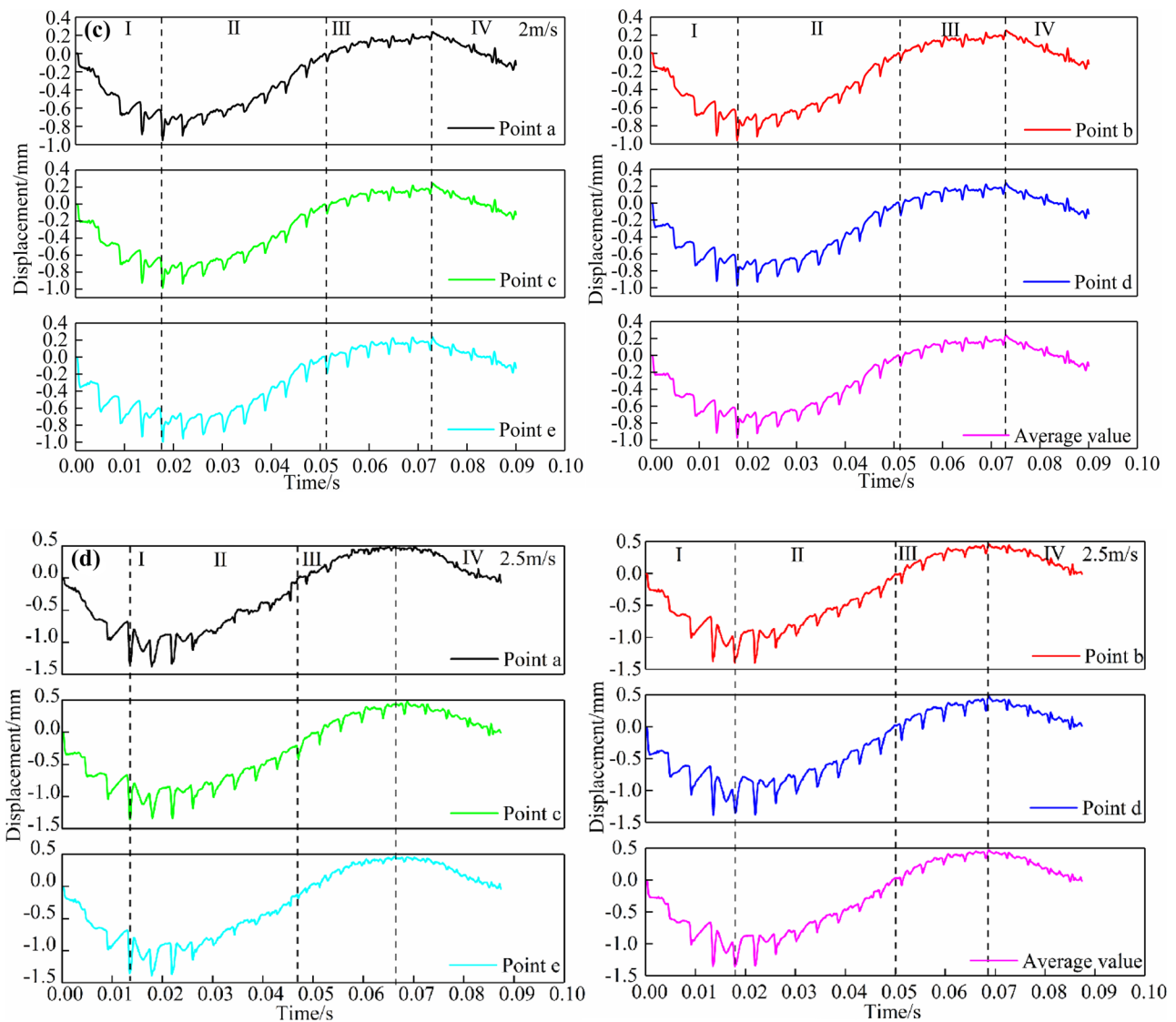


Fig. 10 (continued)

wave propagation. Taking 2.5 m/s impact velocity as an example, the maximum displacement of coal sample surface points a, b, c, d and e during the first wave propagation is -0.129 mm, -0.141 mm, -0.150 mm, -0.167 mm, and -0.188 mm, respectively. The maximum displacement during stress wave propagation is -1.313 mm, -1.335 mm, -1.364 mm, -1.378 mm, and -1.393 mm, respectively. Although the energy carried by the first stress waves is greater than that carried by subsequent stress waves, the multiple effects of stress waves enhance the activation of microcracks in coal samples, weaken their ability to resist stress waves, and increase their deformation ability. Therefore, the subsequent stress wave will lead to greater displacement of the coal sample surface; that is, the deformation of the coal sample in the subsequent stress wave

propagation process is greater than the first wave propagation process.

The horizontal displacement variation laws of coal surface points a, b, c, d, and e were roughly the same under the same impact velocity, but the displacement values differed. In the early stage of stress wave attenuation, the displacement of the point close to the dynamic load source was large, and the displacement of the point away from the dynamic load source was small. Thus, it could be concluded that the displacement of point e was the largest and that of point a was the smallest. At the later stage of stress wave attenuation, the horizontal displacement values at different positions were similar. The point closer to the dynamic load source was preferentially affected by the stress wave in the early stage of attenuation, while the displacement of the point

away from the dynamic load source decreases due to the lag of the position. At the late stage of oscillation, the oscillation propagation of the stress wave gradually stabilized, and the carried energy declined. Therefore, the horizontal displacements at different positions were similar in the later period of oscillation. With the increase of impact velocity, the maximum horizontal displacement value of each point kept increasing, and the horizontal displacement of coal surface points was positively correlated with impact velocity.

Velocity and acceleration of displacement

The displacement of coal surface points does not always increase or decrease but varies in an oscillatory manner. In the complex change process of displacement, the velocity and acceleration of displacement could change dynamically. Analyzing the change of velocity and acceleration of surface point displacement of coal contributed to further explaining the evolution characteristics of displacement. In this paper, Match ID software in the DIC test system was used to analyze the displacement, velocity, and acceleration of coal surface points. The displacement velocity was the first derivative of displacement, and the displacement acceleration was the second derivative (Wang et al. 2021). The changes of displacement velocity and acceleration in the horizontal direction of coal surface points a, b, c, d, and e are shown in Figs. 11 and 12.

The values and directions of horizontal displacement velocity and displacement acceleration at points a, b, c, d, and e on the coal surface changed from time to time (Figs. 11 and 12). Differences occurred in the changes in displacement velocity and acceleration in different stages of displacement. The velocity and acceleration of negative displacement appeared before that of positive displacement with increasing negative displacement oscillation, and the maximum velocity of negative displacement was greater than that of positive displacement, which directly resulted in the negative increase of displacement. The negative displacement velocity gradually decreased when the negative displacement oscillation declined. The acceleration of positive displacement was much greater than that of negative displacement, which explained why the displacement tended to decrease in the negative direction in the form of variable deceleration. The positive displacement velocity and acceleration were larger than the negative ones during the increase of positive displacement oscillation, directly transforming the displacement direction from negative to positive. The velocity and acceleration of displacement were significantly lower than that of displacement in the decreasing period of positive displacement oscillation and later tended to be stabilized, which was also the direct reason for the displacement decrease. Notably, the surface point displacement of coal changed in the form of variable acceleration and velocity.

The variation trends of displacement velocity and displacement acceleration at different positions on the coal surface were similar under the same impact velocity but with different values. With the decrease of the distance from the dynamic load source, the negative and positive displacement velocity and displacement acceleration tended to increase. In other words, the displacement velocity and displacement acceleration of point a were the smallest, and those of point e were the largest, which was similar to the changing trend displacement. Under different impact velocities, the horizontal displacement velocity and acceleration of coal sample surface points differed as well. The negative and positive displacement velocity and displacement acceleration of coal surface point a, b, c, d, and e increase with impact velocity. When the impact velocity was 2.5 m/s, the negative and positive displacement velocity and acceleration reached the maximum. It could be concluded that the horizontal displacement velocity and displacement acceleration of coal surface points were positively correlated with the dynamic load velocity. Furthermore, the largest displacement velocity and acceleration of the coal sample surface occur after the first wave propagation, which is consistent with the displacement evolution law. As a result, the highest deformation of the coal sample surface, as well as the deformation velocity and acceleration, occurs after the first wave propagation.

Multi-fractal characteristics and correlation

The stress wave and the displacement of coal surface points changed in the form of non-linearity and heterogeneity. The multi-fractal theory is effective in studying the non-linear and heterogeneous changes of complex time series characteristic parameters (Lyubushin et al. 2013, 2014). Multi-fractal is defined as an infinite set of fractal measures composed of multiple scaling indices on the fractal structure, which can comprehensively reflect the singularity of complex time series, the degree of heterogeneity, and volatility (Li et al. 2017a, 2020b). If the attenuation of stress wave and the change of horizontal displacement of coal sample surface points have multiple classification characteristics, the distribution law of high-intensity and low-intensity signals in stress wave and the change characteristics of large-scale and small-scale displacement can be analyzed using multi-fractal characteristic parameters. In addition, the correlation between the stress wave and coal surface point displacement can also be revealed based on the correlation between the two multi-fractal characteristic parameters.

Multi-fractal characteristics

The calculation formula of the multi-fractal spectrum is as follows (Li et al. 2017a, 2020b):

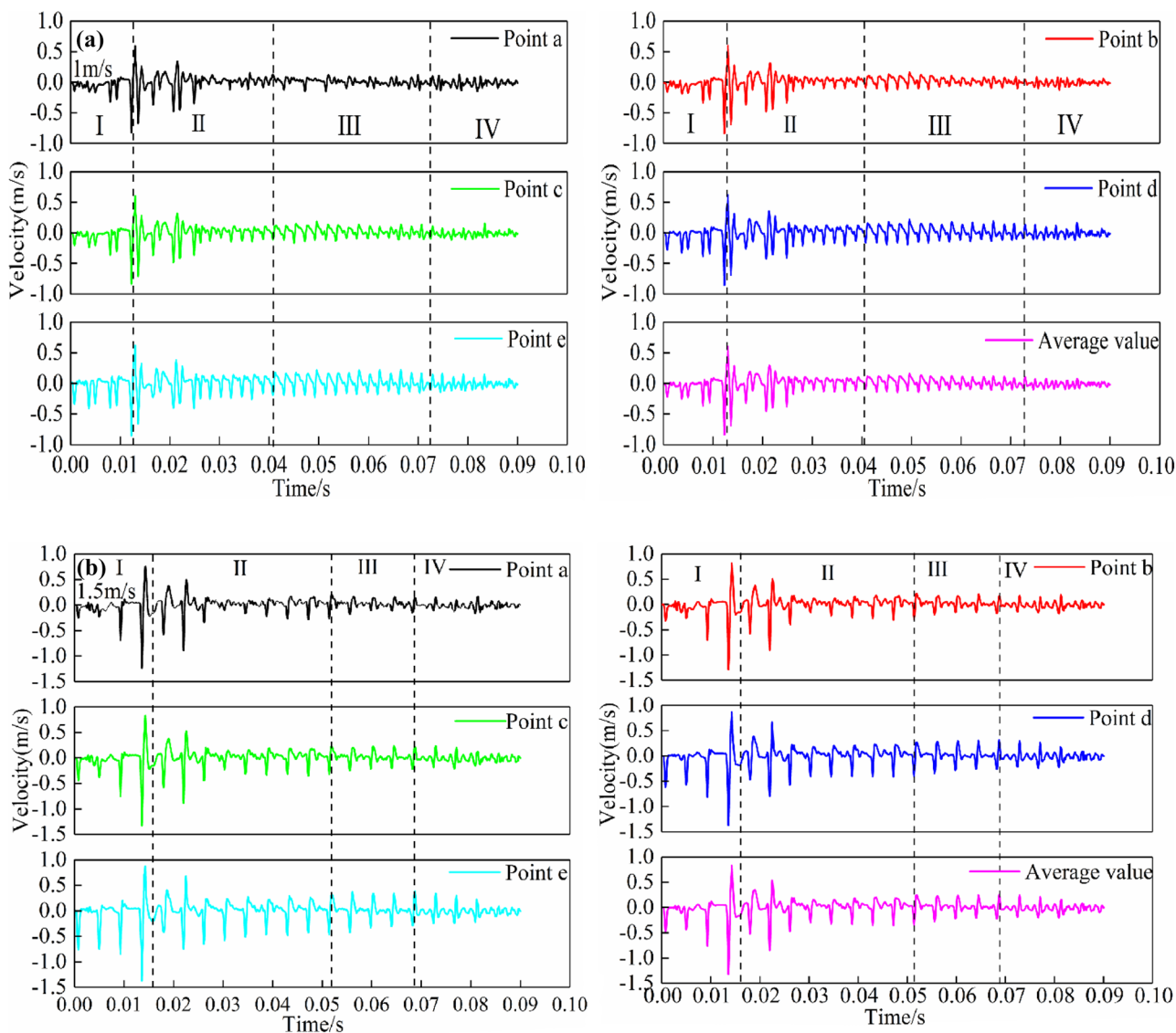


Fig. 11 Displacement velocity (a: 1m/s, b: 1.5m/s, c: 2m/s, d: 2.5m/s)

$$f(\alpha) = \alpha q - \tau(q) \tag{1}$$

where α refers to singularity; $f(\alpha)$ is the frequency of the subset represented by α in the subset set and also the fractal dimension of subset α ; and $\tau(q)$ is the quality index (Li et al. 2021a). The width of the multi-fractal spectrum is defined as follows (Li et al. 2021a):

$$\Delta\alpha = \alpha_{max} - \alpha_{min} \tag{2}$$

where α_{max} represents the small-scale signal subset and α_{min} represents the large-scale signal subset. The width $\Delta\alpha$ of the multi-fractal spectrum can reflect the difference between signals. Larger $\Delta\alpha$ gives rise to a greater difference in signal distribution, representing a greater difference between large-scale and

small-scale signals (Li et al. 2021a). The relationship between the frequency of small-scale and large-scale signals can be obtained through the following equation (Li et al. 2017a, 2020b):

$$\Delta f = f(\alpha_{max}) - f(\alpha_{min}) \tag{3}$$

Smaller Δf corresponds to a larger proportion of large-scale signals, and vice versa. If $\Delta f > 0$, the small-scale signal is dominant; if $\Delta f < 0$, the large-scale signal is dominant (Li et al. 2017a, 2020b).

Before using multi-fractal theory to analyze stress waves and displacements, it is necessary to check whether stress waves and displacements have multi-fractal characteristics. The $\ln Xq(k) - \ln(k)$ curve of stress wave and displacement can prove whether they have multi-fractal (Fig. 13).

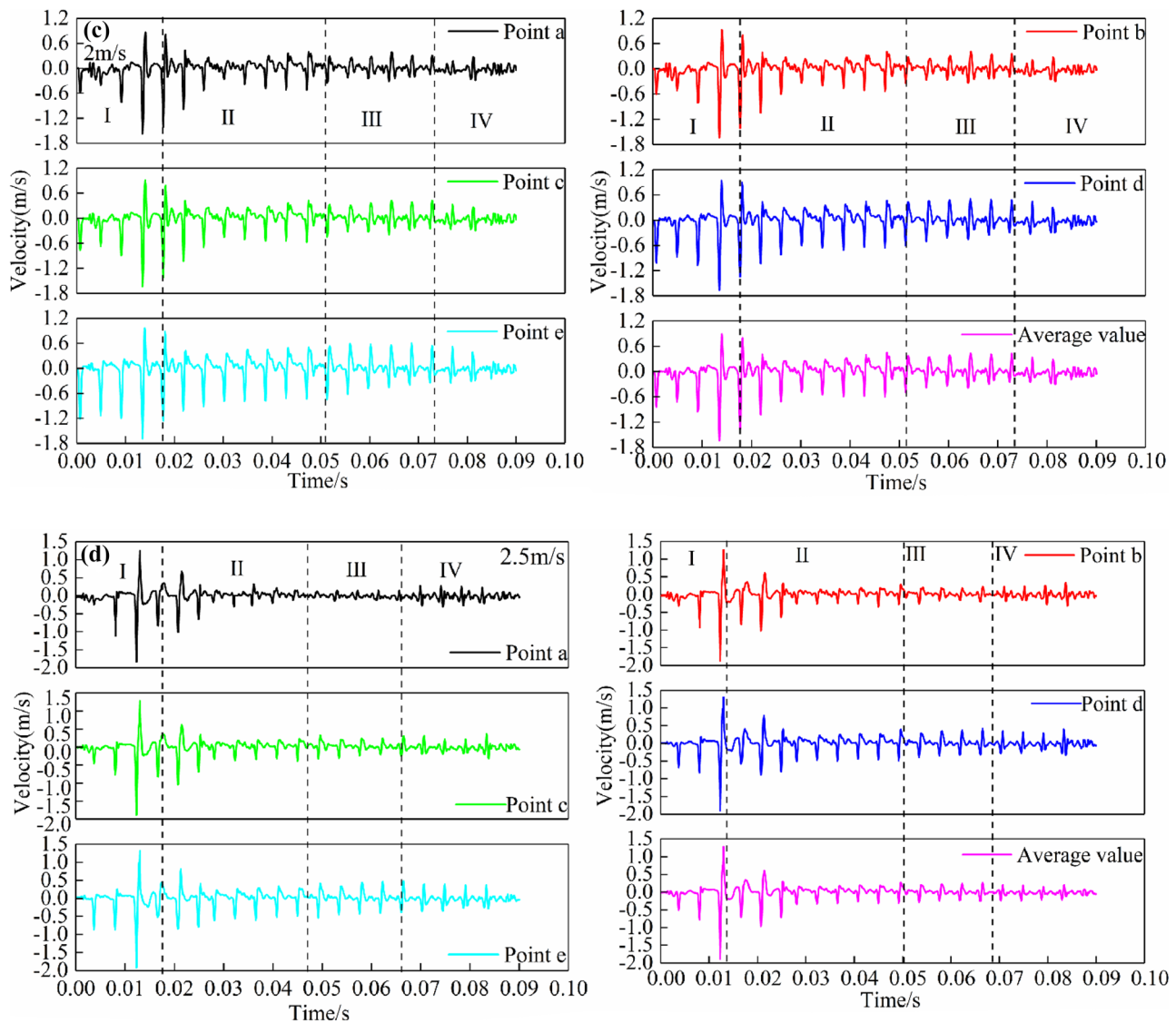


Fig. 11 (continued)

As shown in the Fig. 13, the $\ln Xq(k) - \ln(k)$ curves have a linear relationship and converge at a point, which shows that the time series of stress wave and displacement meet the scaling invariance and have multi-fractal characteristics.

The multiform patterns of incident rod end stress wave P_{IR} and transmitted rod end stress wave P_T and the changes of their characteristic parameters under different impact velocities were shown in Fig. 14).

As shown in Fig. 14, the incident rod end stress wave and transmitted stress wave signals have multi-fractal characteristics. However, obvious differences can be found in the shape and parameters of its multi-fractal spectrum. The multi-fractal spectrum of the stress wave at the incident rod end is “left hook”, and $\Delta\alpha_{IR}$ is greater than 0, but Δf_{IR} is less than 0. The multi-fractal spectrum of transmission wave

is “right hook”, and $\Delta\alpha_T$ and Δf_T are greater than 0. There are huge differences between the high amplitude and low amplitude signals of incident rod end stress waves and transmitted waves. However, the incident rod-end stress waves are dominated by high amplitude signals and the transmitted waves by low amplitude signals. Both similarities and differences can be found in the characteristic parameters of multi-fractal of incident rod end stress waves and transmitted waves under different impact velocities. $\Delta\alpha_{IR}$ of incident rod end stress wave and $\Delta\alpha_T$ of transmitted stress wave increase with impact velocity, which shows that the difference of stress wave time series signals increases with growing impact velocity. In other words, it means larger differences between high and low amplitude signals and more obvious multi-fractal characteristics of stress waves. With

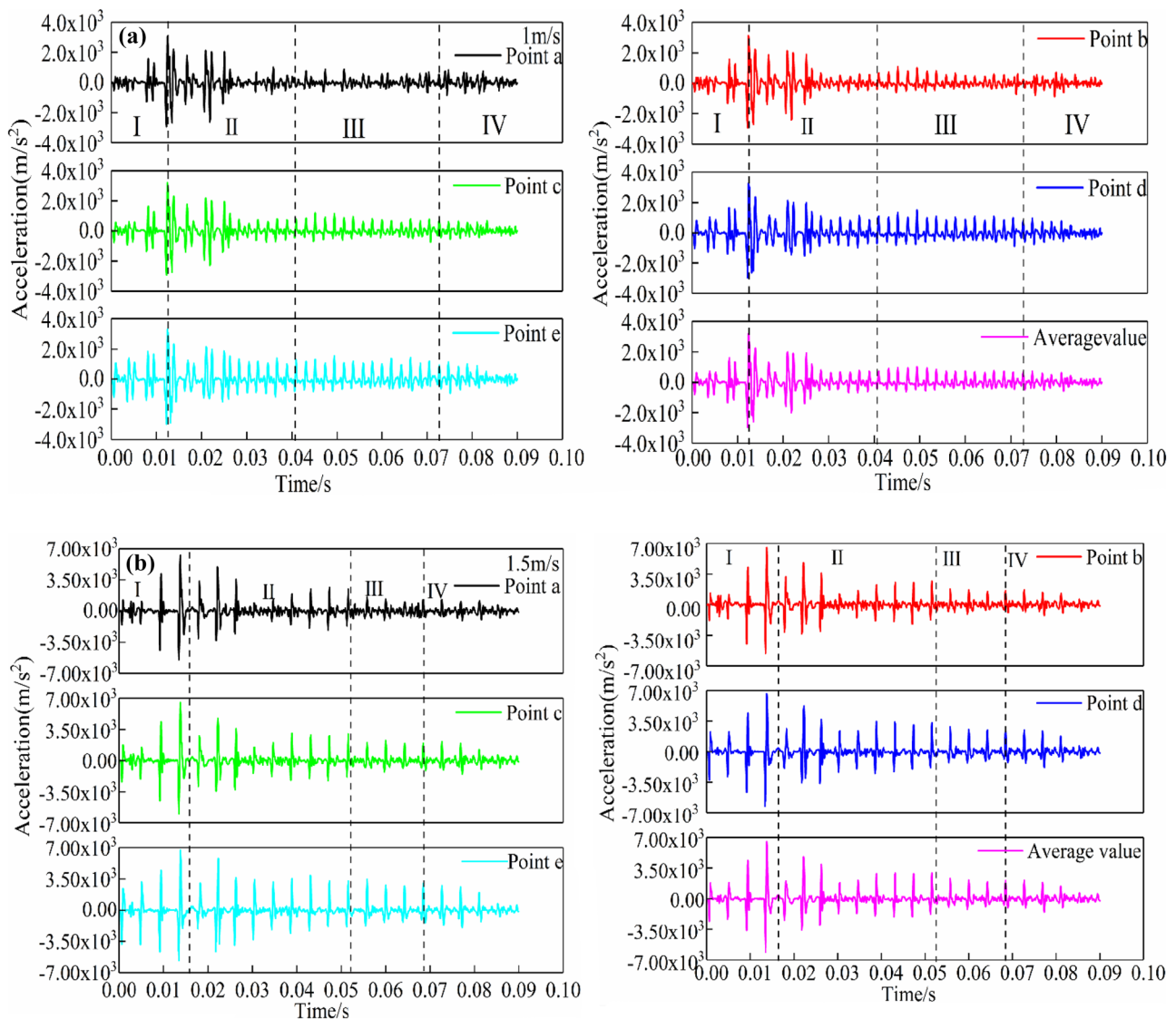


Fig. 12 Displacement acceleration (a: 1m/s, b: 1.5m/s, c: 2m/s, d: 2.5m/s)

the increase of impact velocity, the Δf_{IR} of incident rod end stress wave fluctuates between -0.47 and 0.41 , while the Δf_T of the transmitted wave increases continuously, which shows that the proportion of low and high amplitude signals of incident rod end stress wave is less affected by impact velocity compared with that of the transmitted stress wave.

In the stress wave attenuation process, the multi-fractal characteristics of horizontal displacement of coal sample surface points (a, b, c, d, and e) are shown in Fig. 15.

As shown in Fig. 15, the horizontal displacement of coal sample surface points (a, b, c, d, and e) are multi-fractal, and a “left hook” shaped multi-fractal spectrum, where $\Delta\alpha_D > 0$ and $\Delta f_D < 0$. The fluctuation of horizontal displacement on the surface of the coal sample is strong. Meanwhile, the difference between large-scale and small-scale displacement is

large, with a larger proportion of large-scale displacement. Under the same impact velocity, the multi-fractal characteristic parameters of points a, b, c, d, and e are different. With a shorter distance from the dynamic load source, $\Delta\alpha_D$ decreases continuously. The horizontal displacement fluctuation of the points far away from the dynamic load source and the differences between large-scale and small-scale displacement are relatively large with relatively obvious multi-typing features. The fluctuation of horizontal displacement near the dynamic load source and the difference between large-scale and small-scale displacement are relatively small with weak multi-typing features. With increased impact velocity, large-scale and small-scale displacement differences become larger, with more obvious multi-fractal displacement characteristics. The difference between the

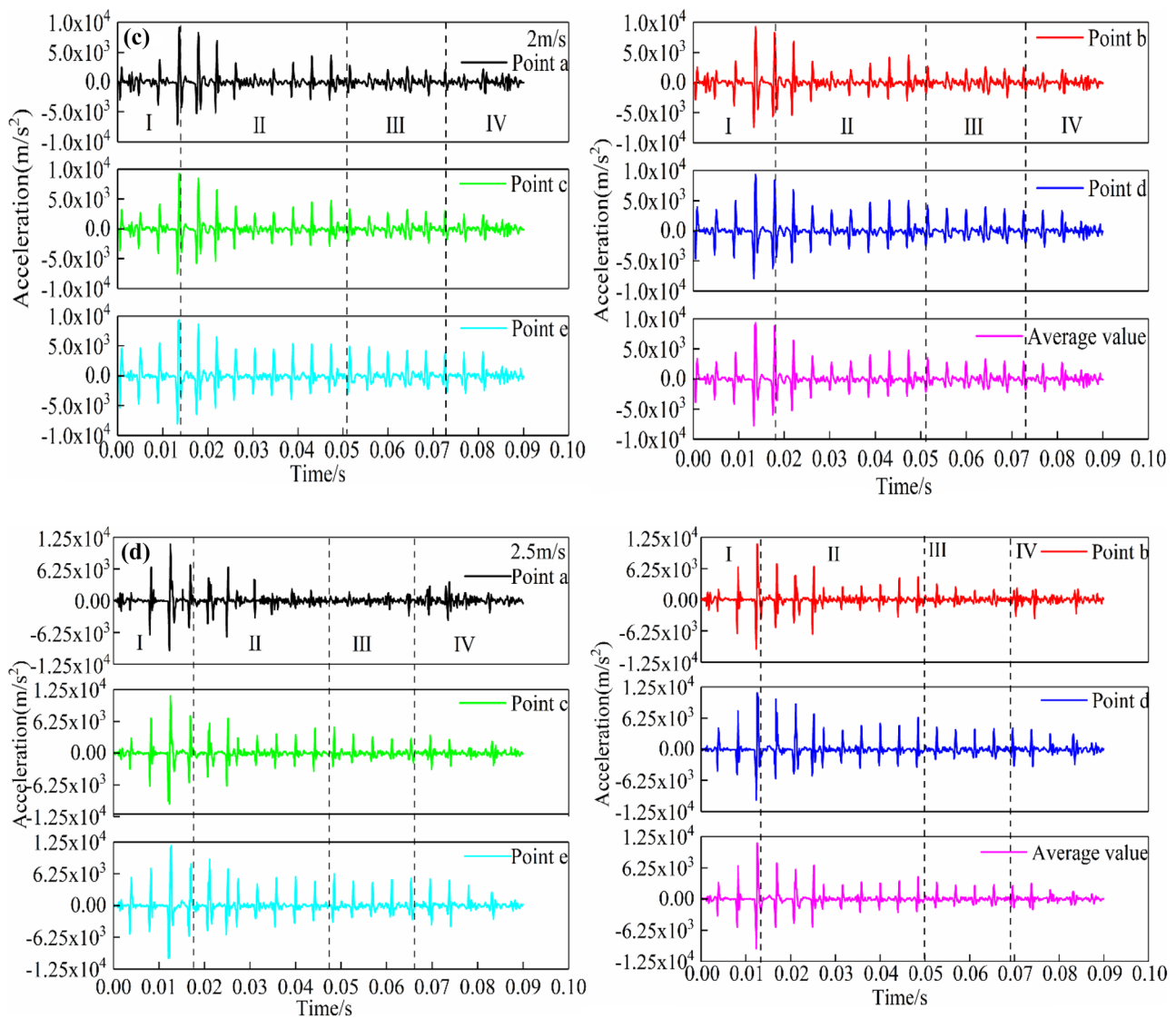


Fig. 12 (continued)

large-scale and small-scale displacement of coal surface particles is positively correlated with impact velocity. As impact velocity increases, the difference experienced an inverted v-shape change (increase first and then decrease). Besides, the proportion of large-scale and small-scale displacement on the coal sample surface shows the same changing trend with increased impact velocity.

Correlation between stress wave and displacement

Figure 16 shows the variation of multi-fractal characteristic parameters of horizontal displacement of points on the coal sample surface with multi-fractal parameters of the stress wave.

With the increase of multi-fractal parameters $\Delta\alpha_{IR}$ and $\Delta\alpha_T$, the $\Delta\alpha_D$ of coal sample surface displacement increases continuously. The fluctuation of horizontal displacement of the coal sample surface is positively correlated with the fluctuation of the dynamic load stress wave. In other words, the difference between large-scale and small-scale displacement is positively correlated with the difference between the high and low amplitude signals of the dynamic load stress wave. When $\Delta\alpha_D$ takes a certain value, which is when the difference between large-scale and small-scale displacement on the coal sample surface is constant, $\Delta\alpha_T$ is much less than $\Delta\alpha_{IR}$. When there is little difference between high and low amplitude signals of the transmitted wave, the difference between large-scale and small-scale displacement will greatly change. However, larger differences are required for

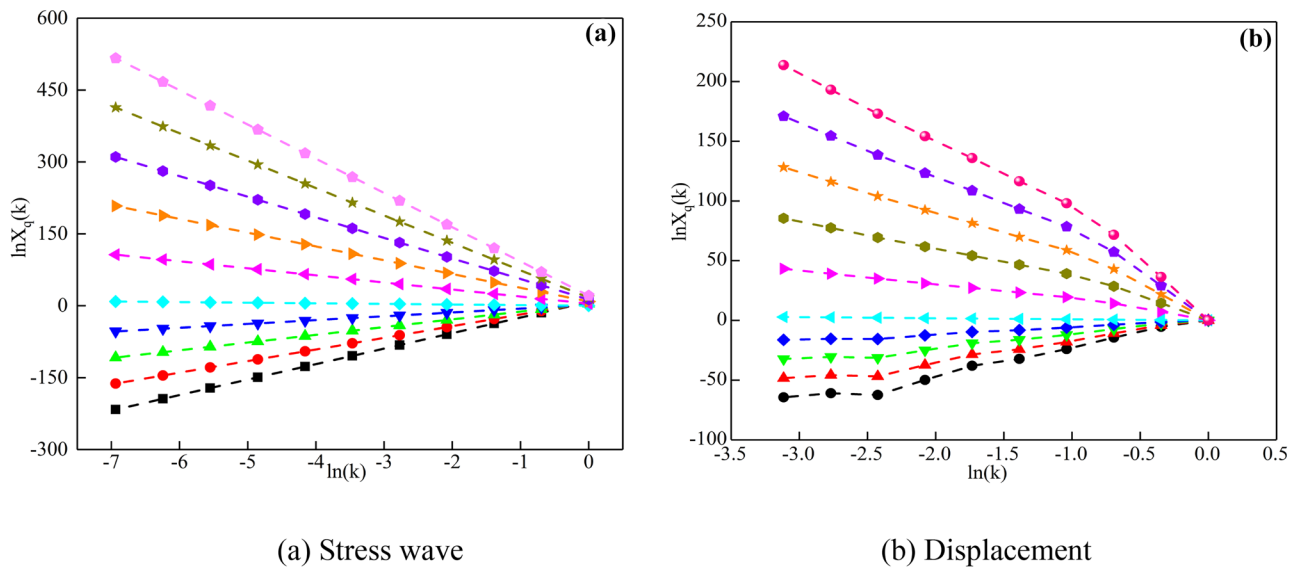


Fig. 13 The relationship between $\ln X_q(k)$ and $\ln(k)$

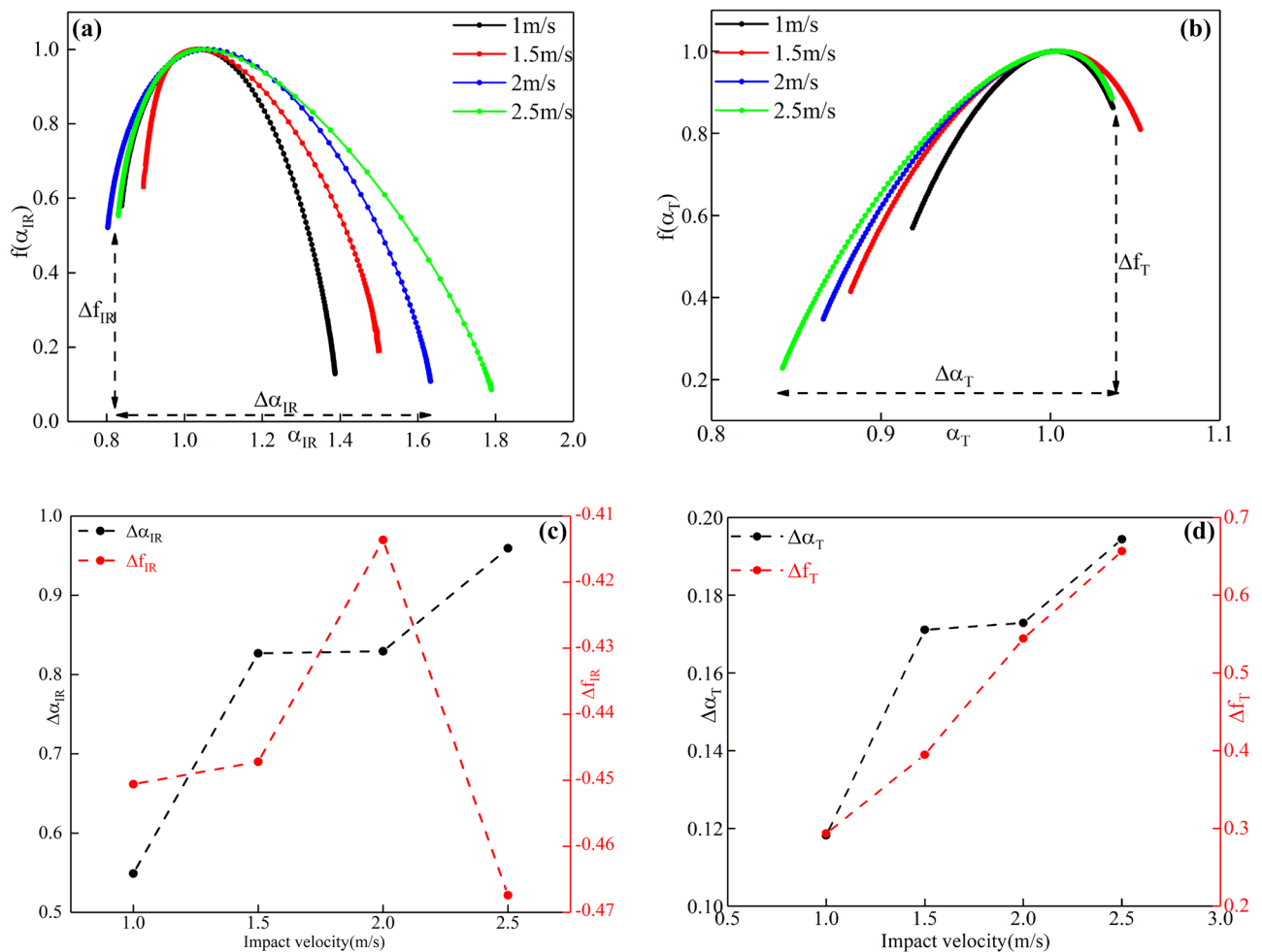


Fig. 14 Multi-fractal characteristics of stress wave (a: Incident rod end stress wave, b: Transmitted rod stress wave, c: the $\Delta\alpha_{IR}$ and Δf_{IR} at different impact velocity, d: the $\Delta\alpha_T$ and Δf_T at different impact velocity)

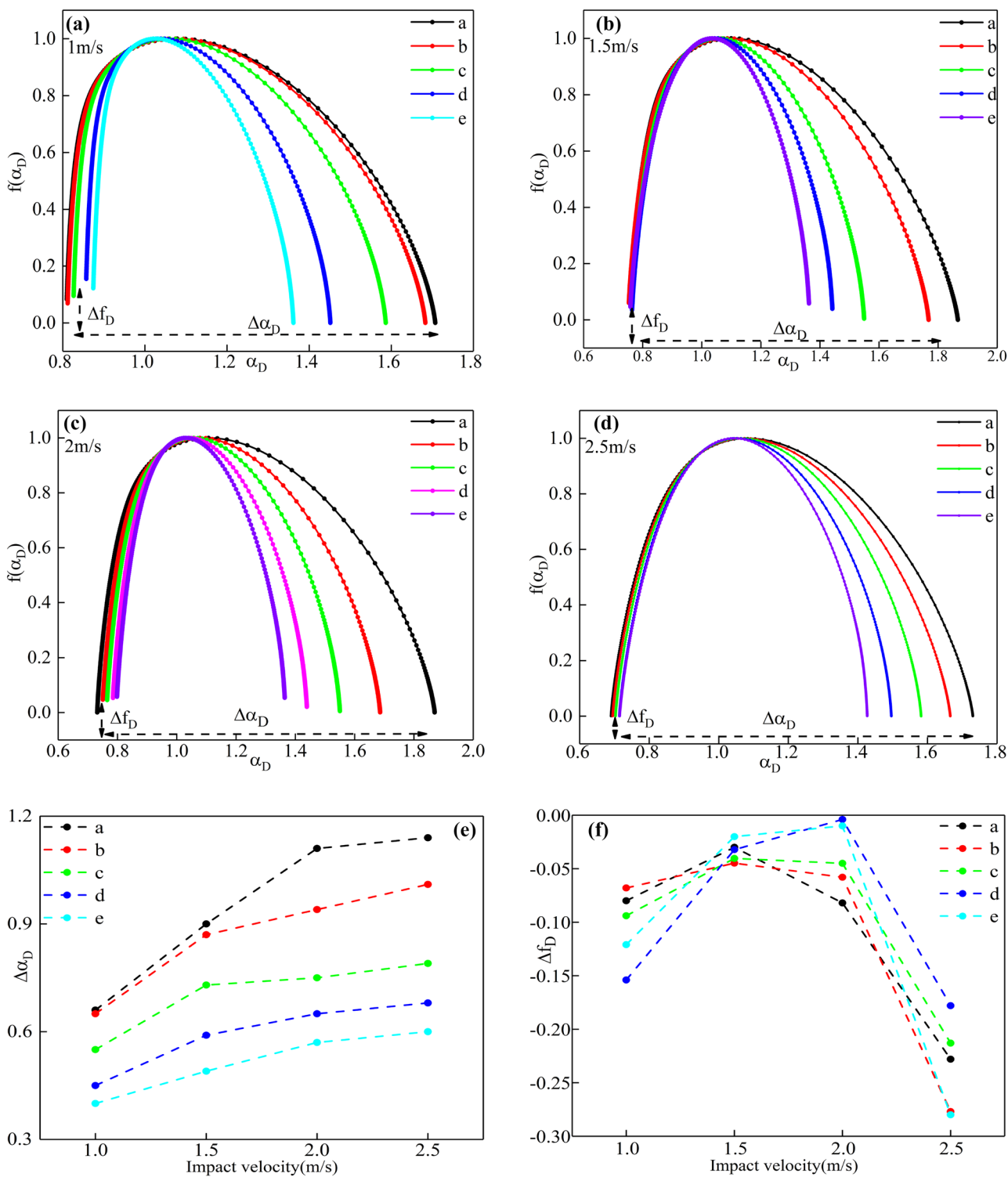


Fig. 15 Multi-fractal parameters of surface point displacement of coal samples (a: 1m/s, b: 1.5m/s, c: 2m/s, d: 2.5m/s, e: the $\Delta\alpha_D$ at different impact velocity, f: the Δf_D at different impact velocity)

the stress wave signal at the incident rod end to bring about the same change of displacement. In the case of the point a, for example, when $\Delta\alpha_D$ is 0.66, $\Delta\alpha_{IR}$ is 0.55, but $\Delta\alpha_T$ is only 0.12. When $\Delta\alpha_D$ increases to 1.14, $\Delta\alpha_{IR}$ is 0.96 and $\Delta\alpha_T$

is only 0.19. The transmission wave has a greater impact on the difference between the large-scale and small-scale displacement of the coal sample surface. With the increase of Δf_{IR} and Δf_T , Δf_D increases first and then decreases. In

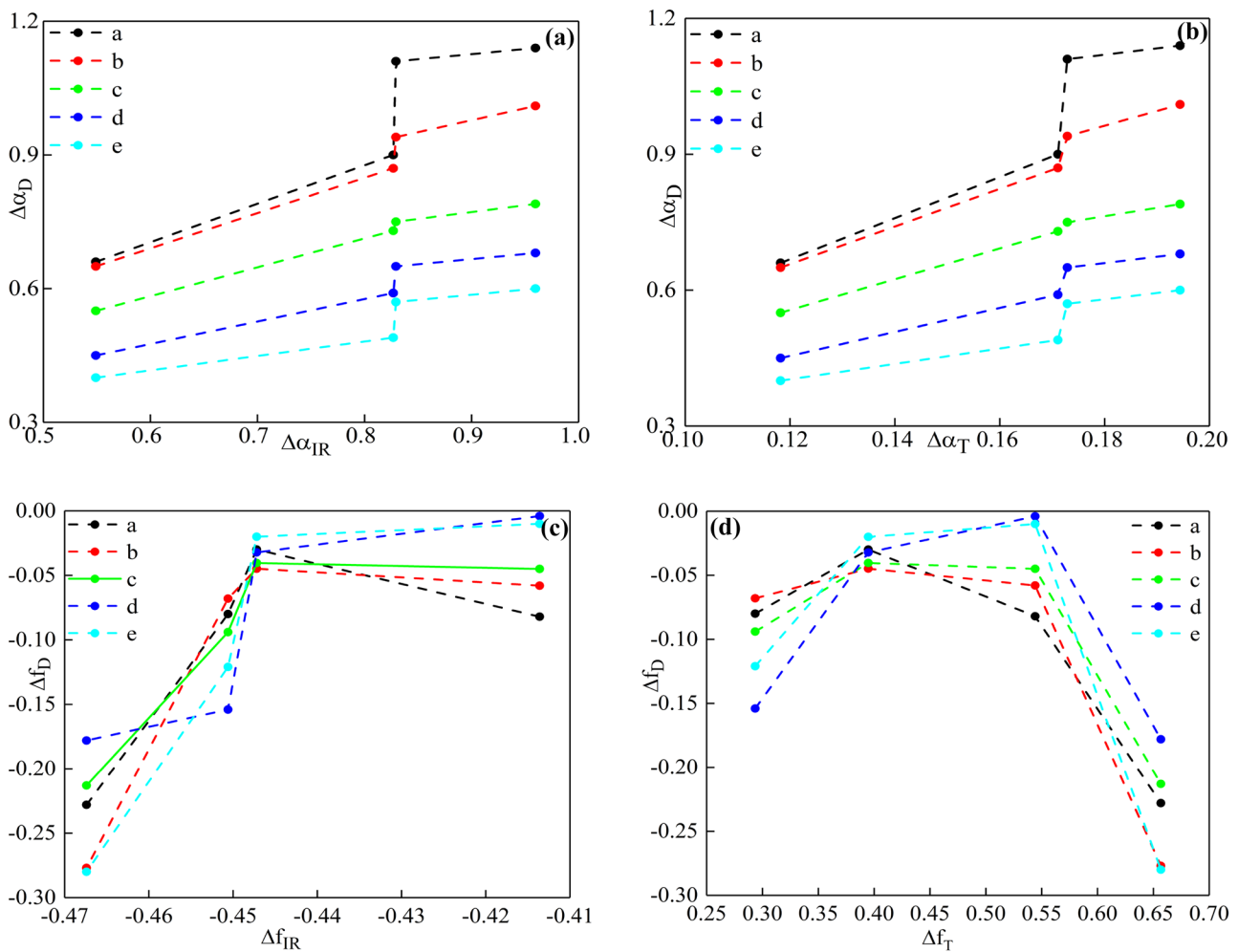


Fig. 16 Correlation characteristics (a: the correlation between $\Delta\alpha_D$ and $\Delta\alpha_{IR}$, b: the correlation between $\Delta\alpha_D$ and $\Delta\alpha_T$, c: the correlation between Δf_D and Δf_{IR} d: the correlation between Δf_D and Δf_T)

a certain range, the high amplitude signal of the stress wave is positively correlated with the large-scale displacement of the coal sample surface. However, when it exceeds the critical value, the high amplitude signal of the stress wave will be negatively correlated with the large-scale displacement of the coal sample surface, which is more obvious in the transmitted wave.

Conclusions

In this paper, the impact experiments of coal were carried out using SHPB and DIC. The author systematically studied the multiple propagation characteristics of the stress wave, evolution patterns of horizontal displacement, displacement velocity, and displacement acceleration of coal under dynamic load. The correlation between dynamic load stress wave and the horizontal displacement of coal surface points

was analyzed based on multi-fractal theory. The detailed conclusions are as follows:

1. The stress wave propagates in the non-linear attenuation mode of multiple incidences, reflections, and transmissions. And the attenuation velocity of the stress wave amplitude also decreases in a non-linear form. Among them, the attenuation velocity of the incident wave is the largest, followed by the attenuation velocity of the reflected wave, and the attenuation velocity of the transmitted wave is the smallest. The incident and reflected stress waves, which are dominated by high amplitude signals and those of transmitted stress waves, are dominated by low amplitude signals. Not only the absolute values of the amplitude of incident, reflected, and transmitted waves are positively correlated with the impact velocity, but also their attenuation velocity is positively correlated with the impact velocity.

2. The horizontal displacement of the coal surface points change in the form of variable velocity and acceleration during the attenuation of the stress wave. And the displacement direction of coal sample surface is dominated by the compression and tension of the stress wave. The change process can be divided into four stages, i.e., two stages of increase and decrease in negative displacement oscillations and two similar stages in positive ones. Among them, the displacement and its rate in the increasing period of negative oscillation are the largest.
3. The stress wave and the surface point displacement of coal have multi-fractal characteristics. Herein, the stress wave at the incident rod end has a “left hook” shaped multi-fractal spectrum with $\Delta\alpha_{IR}$ greater than 0 and Δf_{IR} less than 0. The multi-fractal spectrum shape of transmission wave is “right hook”, with $\Delta\alpha_T$ and Δf_T larger than 0. The multi-fractal spectrum shape of horizontal displacement of the coal sample surface is “left hook type” with $\Delta\alpha_D > 0$ but $\Delta f_D < 0$. According to the characteristic parameters of multi-fractal, the high amplitude signal accounts for a larger proportion in the incident rod end stress wave, while the low amplitude one accounts for a larger proportion in the transmitted wave. The large-scale displacement determines point displacement on the surface of coal samples. The proportional relationship and difference between large-scale and small-scale displacement are affected by those between high and low amplitude signals of the stress wave, and the influence of the transmission wave is greater.

Acknowledgements This project is supported by the Postgraduate Research & Practice Innovation Program of Jiangsu Province (KYCX22_2659), the Graduate Innovation Program of China University of Mining and Technology (2022WLKXJ099), the National Science Foundation for Young Scientists of Jiangsu Province (BK20180644), and the National Natural Science Foundation of China (52004267, 52104231).

Author contribution Xiaoliang Li: Methodology, Formal analysis, Visualization, Writing-Original draft preparation.

Enlai Zhao: Conceptualization, Resources, Funding acquisition.

Zhentang Liu: Funding acquisition, Project administration, Supervision.

Yubing Liu: Software, Validation.

Xiaojun Feng: Validation, Data Curation.

Zhoujie Gu: Investigation, Writing-Reviewing and Editing.

Declarations

Conflict of interest The authors declare no competing interests.

References

Ai D, Zhao Y, Wang Q, Li C (2019) Experimental and numerical investigation of crack propagation and dynamic properties of rock in

- SHPB indirect tension test. *Int J Impact Eng* 126:135–146. <https://doi.org/10.1016/j.ijimpeng.2019.01.001>
- Ai D, Zhao Y, Wang Q, Li C (2020) Crack propagation and dynamic properties of coal under SHPB impact loading: Experimental investigation and numerical simulation. *Theor Appl Fract Mech* 105:102393. <https://doi.org/10.1016/j.tafmec.2019.102393>
- Chai SB, Li JC, Zhang QB et al (2016) Stress wave propagation across a rock mass with two non-parallel joints. *Rock Mech Rock Eng* 49:4023–4032. <https://doi.org/10.1007/s00603-016-1068-z>
- Chen R, Xia K, Dai F et al (2009) Determination of dynamic fracture parameters using a semi-circular bend technique in split Hopkinson pressure bar testing. *Eng Fract Mech* 76:1268–1276. <https://doi.org/10.1016/j.engfracmech.2009.02.001>
- Cheng Y, Song Z, Jin J et al (2019) Experimental study on stress wave attenuation and energy dissipation of sandstone under full deformation condition. *Arab J Geosci* 12:736. <https://doi.org/10.1007/s12517-019-4915-x>
- Cong Y, Zhai C, Sun Y et al (2021) Visualized study on the mechanism of temperature effect on coal during liquid nitrogen cold shock. *Appl Therm Eng* 194:116988. <https://doi.org/10.1016/j.applthermaleng.2021.116988>
- Dai F, Chen R, Xia K (2010) A Semi-Circular Bend Technique for Determining Dynamic Fracture Toughness. *Exp Mech* 50:783–791. <https://doi.org/10.1007/s11340-009-9273-2>
- Fakhimi A, Lin Q, Labuz JF (2018) Insights on rock fracture from digital imaging and numerical modeling. *Int J Rock Mech Min Sci* 107:201–207. <https://doi.org/10.1016/j.ijrmmms.2018.05.002>
- Feng J, Wang E, Shen R et al (2016) A source generation model for near-field seismic impact of coal fractures in stress concentration zones. *J Geophys Eng* 13:516–525. <https://doi.org/10.1088/1742-2132/13/4/516>
- Feng J, Wang E, Huang Q et al (2020a) Experimental and numerical study of failure behavior and mechanism of coal under dynamic compressive loads. *Int J Min Sci Technol* 30:613–621. <https://doi.org/10.1016/j.ijmst.2020.06.004>
- Feng X, Zhang Q, Wang E et al (2020b) 3D modeling of the influence of a splay fault on controlling the propagation of nonlinear stress waves induced by blast loading. *Soil Dyn Earthq Eng* 138:106335. <https://doi.org/10.1016/j.soildyn.2020.106335>
- Gao G, Huang S, Xia K, Li Z (2015) Application of digital image correlation (DIC) in dynamic notched semi-circular bend (NSCB) tests. *Exp Mech* 55:95–104. <https://doi.org/10.1007/s11340-014-9863-5>
- Golewski GL (2021) Evaluation of fracture processes under shear with the use of DIC technique in fly ash concrete and accurate measurement of crack path lengths with the use of a new crack tip tracking method. *Measurement* 181:109632. <https://doi.org/10.1016/j.measurement.2021.109632>
- Gu Z, Shen R, Liu Z, Zhao E, Chen H, Yuan Z, Chu X, Tian J (2023) Dynamic characteristics of coal under triaxial constraints based on the Split-Hopkinson pressure bar test system. *Nat Resour Res* 32(2):587–601. <https://doi.org/10.1007/s11053-022-10152-6>
- Han Z, Li D, Li X (2022) Dynamic mechanical properties and wave propagation of composite rock-mortar specimens based on SHPB tests. *Int J Min Sci Technol* 32:793–806. <https://doi.org/10.1016/j.ijmst.2022.05.008>
- Hao X, Du W, Zhao Y et al (2020) Dynamic tensile behaviour and crack propagation of coal under coupled static-dynamic loading. *Int J Min Sci Technol* 30:659–668. <https://doi.org/10.1016/j.ijmst.2020.06.007>
- Hong L, Zhou Z, Yin T et al (2009) Energy consumption in rock fragmentation at intermediate strain rate. *J Cent South Univ Technol* 16:677–682. <https://doi.org/10.1007/s11771-009-0112-5>
- Hou S, Liang S, Liu D (2023) Study on dynamic mechanical properties and constitutive model of granite under constant strain rate loading. *Constr Build Mater* 363:129975. <https://doi.org/10.1016/j.conbuildmat.2022.129975>

- Huang S, Xia K, Yan F, Feng X (2010) An experimental study of the rate dependence of tensile strength softening of Longyou sandstone. *Rock Mech Rock Eng* 43:677–683. <https://doi.org/10.1007/s00603-010-0083-8>
- Jobin TM, Ramji M, Khaderi SN (2021) A comparison of domain integral and multi-parameter methods for the strain intensity factor estimation of rigid line inclusion using digital image correlation. *Theor Appl Fract Mech* 115:103064. <https://doi.org/10.1016/j.tafmec.2021.103064>
- Ju Y, Sudak L, Xie H (2007) Study on stress wave propagation in fractured rocks with fractal joint surfaces. *Int J Solids Struct* 44:4256–4271. <https://doi.org/10.1016/j.ijsolstr.2006.11.015>
- Kai-Xin L, Xu-Dong L (2006) A new method for separation of waves in improving the conventional SHPB technique. *Chinese Phys Lett* 23:3045–3048. <https://doi.org/10.1088/0256-307X/23/11/044>
- Kong X, Wang E, Li S et al (2020) Dynamic mechanical characteristics and fracture mechanism of gas-bearing coal based on SHPB experiments. *Theor Appl Fract Mech* 105:102395. <https://doi.org/10.1016/j.tafmec.2019.102395>
- Kong X, Li S, Wang E et al (2021a) Dynamics behaviour of gas-bearing coal subjected to SHPB tests. *Compos Struct* 256:113088. <https://doi.org/10.1016/j.compstruct.2020.113088>
- Kong X, Li S, Wang E et al (2021b) Experimental and numerical investigations on dynamic mechanical responses and failure process of gas-bearing coal under impact load. *Soil Dyn Earthq Eng* 142:106579. <https://doi.org/10.1016/j.soildyn.2021.106579>
- Kong X, He D, Liu X et al (2022) Strain characteristics and energy dissipation laws of gas-bearing coal during impact fracture process. *Energy* 242:123028. <https://doi.org/10.1016/j.energy.2021.123028>
- Lai D, Demartino C, Xiao Y (2022) High-strain rate tension behavior of fiber-reinforced rubberized concrete. *Cem Concr Compos* 131:104554. <https://doi.org/10.1016/j.cemconcomp.2022.104554>
- Li J, Ma G (2010) Analysis of blast wave interaction with a rock joint. *Rock Mech Rock Eng* 43:777–787. <https://doi.org/10.1007/s00603-009-0062-0>
- Li X, Zhou Z, Lok T-S et al (2008) Innovative testing technique of rock subjected to coupled static and dynamic loads. *Int J Rock Mech Min Sci* 45:739–748. <https://doi.org/10.1016/j.ijrmms.2007.08.013>
- Li J, Ma G, Zhao J (2011a) Stress wave interaction with a nonlinear and slippery rock joint. *Int J Rock Mech Min Sci* 48:493–500. <https://doi.org/10.1016/j.ijrmms.2010.11.013>
- Li Y, Zhu Z, Li B et al (2011b) Study on the transmission and reflection of stress waves across joints. *Int J Rock Mech Min Sci* 48:364–371. <https://doi.org/10.1016/j.ijrmms.2011.01.002>
- Li M, Mao X, Cao L et al (2016) Effects of thermal treatment on the dynamic mechanical properties of coal measures sandstone. *Rock Mech Rock Eng* 49:3525–3539. <https://doi.org/10.1007/s00603-016-0981-5>
- Li B, Li N, Wang E et al (2017a) Characteristics of coal mining micro-seismic and blasting signals at Qianqiu coal mine. *Environ Earth Sci* 76:722. <https://doi.org/10.1007/s12665-017-7070-2>
- Li JC, Li NN, Li HB, Zhao J (2017b) An SHPB test study on wave propagation across rock masses with different contact area ratios of joint. *Int J Impact Eng* 105:109–116. <https://doi.org/10.1016/j.ijimpeng.2016.12.011>
- Li D, Han Z, Zhu Q et al (2019a) Stress wave propagation and dynamic behavior of red sandstone with single bonded planar joint at various angles. *Int J Rock Mech Min Sci* 117:162–170. <https://doi.org/10.1016/j.ijrmms.2019.03.011>
- Li JC, Rong LF, Li HB, Hong SN (2019b) An SHPB test study on stress wave energy attenuation in jointed rock masses. *Rock Mech Rock Eng* 52:403–420. <https://doi.org/10.1007/s00603-018-1586-y>
- Li D, Gao F, Han Z, Zhu Q (2020a) Full- and local-field strain evolution and fracture behavior of precracked granite under coupled static and dynamic loads. *Shock Vib* 2020:1–15. <https://doi.org/10.1155/2020/8866673>
- Li N, Li B, Chen D et al (2020b) Waveform characteristics of earthquakes induced by hydraulic fracturing and mining activities: comparison with those of natural earthquakes. *Nat Resour Res* 29:3653–3674. <https://doi.org/10.1007/s11053-020-09699-z>
- Li B, Wang E, Li Z et al (2021a) Discrimination of different blasting and mine microseismic waveforms using FFT, SPWVD and multifractal method. *Environ Earth Sci* 80:36. <https://doi.org/10.1007/s12665-020-09330-7>
- Li N, Zhou Y, Li H (2021b) Experimental study for the effect of joint surface characteristics on stress wave propagation. *Geomech Geophys Geo-Energ Geo-Resour* 7:50. <https://doi.org/10.1007/s40948-021-00235-8>
- Li X, Liu Z, Feng X et al (2021c) Effects of acid sulfate and chloride ion on the pore structure and mechanical properties of sandstone under dynamic loading. *Rock Mech Rock Eng* 54:6105–6121. <https://doi.org/10.1007/s00603-021-02612-x>
- Li H, Qiao Y, Shen R, He M (2022a) Electromagnetic radiation signal monitoring and multi-fractal analysis during uniaxial compression of water-bearing sandstone. *Measurement* 196:111245. <https://doi.org/10.1016/j.measurement.2022.111245>
- Li Y, Dai F, Liu Y, Wei M (2022b) Experimental evaluation of the transient propagation fracture properties of rocks under dynamic mode I loading: an insight from digital image correlation. *Theor Appl Fract Mech* 119:103370. <https://doi.org/10.1016/j.tafmec.2022.103370>
- Li X, Liu Z, Zhao E et al (2023) Experimental study on the damage evolution behavior of coal under dynamic Brazilian splitting tests based on the Split Hopkinson pressure bar and the digital image correlation. *Nat Resour Res* 32:1435–1457. <https://doi.org/10.1007/s11053-023-10197-1>
- Liu X, Dai F, Zhang R, Liu J (2015) Static and dynamic uniaxial compression tests on coal rock considering the bedding directivity. *Environ Earth Sci* 73:5933–5949. <https://doi.org/10.1007/s12665-015-4106-3>
- Liu K, Zhang QB, Wu G et al (2019) Dynamic mechanical and fracture behaviour of sandstone under multiaxial loads using a triaxial Hopkinson bar. *Rock Mech Rock Eng* 52:2175–2195. <https://doi.org/10.1007/s00603-018-1691-y>
- Liu J, Li Q, Wang X et al (2022a) Dynamic multifractal characteristics of acoustic emission about composite coal-rock samples with different strength rock. *Chaos, Solitons Fractals* 164:112725. <https://doi.org/10.1016/j.chaos.2022.112725>
- Liu Y, Lebedev M, Zhang Y et al (2022b) Micro-cleat and permeability evolution of anisotropic coal during directional CO₂ flooding: an in situ micro-CT study. *Nat Resour Res* 31:2805–2818. <https://doi.org/10.1007/s11053-022-10102-2>
- Liu Y, Wang E, Li M et al (2023) Mechanical response and gas flow characteristics of pre-drilled coal subjected to true triaxial stresses. *Gas Sci Eng* 111:204927. <https://doi.org/10.1016/j.jgsce.2023.204927>
- Lu Y, Zhang S, Gao M et al (2017) Experimental study on energy dissipation of dynamic fracture characteristics of P-CCNBD rock specimens under multiple stress waves. *Chin J Rock Mech Eng* 37:1106–1114. <https://doi.org/10.13722/j.cnki.jrme.2017.1149>
- Lyubushin AA, Kaláb Z, Lednická M, Haggag HM (2013) Discrimination of earthquakes and explosions using multi-fractal singularity spectrums properties. *J Seismol* 17:975–983. <https://doi.org/10.1007/s10950-013-9366-3>
- Lyubushin AA, Kaláb Z, Lednická M (2014) Statistical properties of seismic noise measured in underground spaces during seismic swarm. *Acta Geod Geophys* 49:209–224. <https://doi.org/10.1007/s40328-014-0051-y>

- Ma GW, Li JC, Zhao J (2011) Three-phase medium model for filled rock joint and interaction with stress waves. *Int J Numer Anal Meth Geomech* 35:97–110. <https://doi.org/10.1002/nag.941>
- Ma D, Ma Q, Yuan P (2017) SHPB tests and dynamic constitutive model of artificial frozen sandy clay under confining pressure and temperature state. *Cold Reg Sci Technol* 136:37–43. <https://doi.org/10.1016/j.coldregions.2017.01.004>
- Mondal D, Roy PNS (2019) Fractal and seismic b-value study during dynamic roof displacements (roof fall and surface blasting) for enhancing safety in the longwall coal mines. *Eng Geol* 253:184–204. <https://doi.org/10.1016/j.enggeo.2019.03.018>
- Niu Y, Li Z, Wang E et al (2022) An experimental study on precursor identification for gas-bearing coal failure from electric potential responses in the loading process. *Measurement* 196:111229. <https://doi.org/10.1016/j.measurement.2022.111229>
- Tan L, Ren T, Yang X, He X (2018) A numerical simulation study on mechanical behaviour of coal with bedding planes under coupled static and dynamic load. *Int J Min Sci Technol* 28:791–797. <https://doi.org/10.1016/j.ijmst.2018.08.009>
- Tan L, Ren T, Dou L et al (2021) Dynamic response and fracture evolution of marble specimens containing rectangular cavities subjected to dynamic loading. *Bull Eng Geol Environ* 80:7701–7716. <https://doi.org/10.1007/s10064-021-02425-w>
- Tian H, Li Z, Yin S et al (2023) Research on infrared radiation response and energy dissipation characteristics of sandstone crushing under impact load. *Eng Geol* 107171. <https://doi.org/10.1016/j.enggeo.2023.107171>
- Vardar O, Wei C, Zhang C, Canbulat I (2022) Numerical investigation of impacts of geological faults on coal burst proneness during roadway excavation. *Bull Eng Geol Environ* 81:2. <https://doi.org/10.1007/s10064-021-02508-8>
- Wang P, Luan H (2022) Size effect analysis of remaining coal pillar on rock burst caused by fault. *Bull Eng Geol Environ* 81:108. <https://doi.org/10.1007/s10064-022-02611-4>
- Wang W, Cheng Y, Wang H et al (2015) Fracture failure analysis of hard-thick sandstone roof and its controlling effect on gas emission in underground ultra-thick coal extraction. *Eng Fail Anal* 54:150–162. <https://doi.org/10.1016/j.engfailanal.2015.04.016>
- Wang H, Jiang Y, Xue S et al (2017) Investigation of intrinsic and external factors contributing to the occurrence of coal bumps in the mining area of western Beijing, China. *Rock Mech Rock Eng* 50:1033–1047. <https://doi.org/10.1007/s00603-016-1146-2>
- Wang X, Li S, Xu Z et al (2019) An interval fuzzy comprehensive assessment method for rock burst in underground caverns and its engineering application. *Bull Eng Geol Environ* 78:5161–5176. <https://doi.org/10.1007/s10064-018-01453-3>
- Wang F, Xia K, Yao W et al (2021) Slip behavior of rough rock discontinuity under high velocity impact: Experiments and models. *Int J Rock Mech Min Sci* 144:104831. <https://doi.org/10.1016/j.ijrmms.2021.104831>
- Wu W, Li JC, Zhao J (2014) Role of filling materials in a P-wave interaction with a rock fracture. *Eng Geol* 172:77–84. <https://doi.org/10.1016/j.enggeo.2014.01.007>
- Wu Y, Gao F, Chen J, He J (2019) Experimental study on the performance of rock bolts in coal burst-prone mines. *Rock Mech Rock Eng* 52:3959–3970. <https://doi.org/10.1007/s00603-019-01794-9>
- Xia K, Nasser MHB, Mohanty B et al (2008) Effects of microstructures on dynamic compression of Barre granite. *Int J Rock Mech Min Sci* 45:879–887. <https://doi.org/10.1016/j.ijrmms.2007.09.013>
- Xing T, Zhu H, Wang L et al (2020) High accuracy measurement of heterogeneous deformation field using spatial-temporal subset digital image correlation. *Measurement* 156:107605. <https://doi.org/10.1016/j.measurement.2020.107605>
- Yan Z, Dai F, Zhu J, Xu Y (2021) Dynamic cracking behaviors and energy evolution of multi-flawed rocks under static pre-compression. *Rock Mech Rock Eng* 54:5117–5139. <https://doi.org/10.1007/s00603-021-02564-2>
- Yang Z, Liu C, Zhu H et al (2019) Mechanism of rock burst caused by fracture of key strata during irregular working face mining and its prevention methods. *Int J Min Sci Technol* 29:889–897. <https://doi.org/10.1016/j.ijmst.2018.07.005>
- Yang E, Lin H, Li S et al (2022) Characteristic strength and energy evolution law of coal treated by ultrasonic wave with different power under uniaxial compression. *Nat Resour Res*. <https://doi.org/10.1007/s11053-022-10015-0>
- Yang H, Wang E, Cheng D, Wang X, Li B, Song Y, Wang D, Liu W (2023) Characteristics of energy evolution and acoustic emission response of concrete under the action of acidic drying-saturation processes cycle. *J Build Eng* 74:106928. <https://doi.org/10.1016/j.jobbe.2023.106928>
- Yao W, Xia K, Zhang T (2019) Dynamic fracture test of Laurentian granite subjected to hydrostatic pressure. *Exp Mech* 59:245–250. <https://doi.org/10.1007/s11340-018-00437-4>
- Yu Y, Xin R, Zeng W, Liu W (2021) Fracture resistance curves of wood in the longitudinal direction using digital image correlation technique. *Theor Appl Fract Mech* 114:102997. <https://doi.org/10.1016/j.tafmec.2021.102997>
- Yue Z, Peng L, Qiao Y et al (2022) Dynamic brittle fracture in sharp V-notched rock specimens using digital image correlation method. *Theor Appl Fract Mech* 119:103323. <https://doi.org/10.1016/j.tafmec.2022.103323>
- Zhang QB, Zhao J (2013) Determination of mechanical properties and full-field strain measurements of rock material under dynamic loads. *Int J Rock Mech Min Sci* 60:423–439. <https://doi.org/10.1016/j.ijrmms.2013.01.005>
- Zhang X, Li Z, Wang E et al (2021) Experimental investigation of pressure stimulated currents and acoustic emissions from sandstone and gabbro samples subjected to multi-stage uniaxial loading. *Bull Eng Geol Environ* 80:7683–7700. <https://doi.org/10.1007/s10064-021-02421-0>
- Zhao Y, Zhao G-F, Jiang Y et al (2014) Effects of bedding on the dynamic indirect tensile strength of coal: Laboratory experiments and numerical simulation. *Int J Coal Geol* 132:81–93. <https://doi.org/10.1016/j.coal.2014.08.007>
- Zhao Y, Liu S, Jiang Y et al (2016) Dynamic tensile strength of coal under dry and saturated conditions. *Rock Mech Rock Eng* 49:1709–1720. <https://doi.org/10.1007/s00603-015-0849-0>
- Zhao Y, Gong S, Hao X et al (2017) Effects of loading rate and bedding on the dynamic fracture toughness of coal: laboratory experiments. *Eng Fract Mech* 178:375–391. <https://doi.org/10.1016/j.engfracmech.2017.03.011>
- Zhao T, Guo W, Tan Y et al (2018) Case histories of rock bursts under complicated geological conditions. *Bull Eng Geol Environ* 77:1529–1545. <https://doi.org/10.1007/s10064-017-1014-7>
- Zhou XP, Qian QH, Yang HQ (2011) Rock burst of deep circular tunnels surrounded by weakened rock mass with cracks. *Theoret Appl Fract Mech* 56:79–88. <https://doi.org/10.1016/j.tafmec.2011.10.003>
- Zhou L, Xu S, Shan J et al (2018) Heterogeneity in deformation of granite under dynamic combined compression/shear loading. *Mech Mater* 123:1–18. <https://doi.org/10.1016/j.mechmat.2018.04.013>
- Zhou K, Dou L, Li X et al (2022) Coal burst and mining-induced stress evolution in a deep isolated main entry area – a case study. *Eng Fail Anal* 137:106289. <https://doi.org/10.1016/j.engfailanal.2022.106289>

Springer Nature or its licensor (e.g. a society or other partner) holds exclusive rights to this article under a publishing agreement with the author(s) or other rightsholder(s); author self-archiving of the accepted manuscript version of this article is solely governed by the terms of such publishing agreement and applicable law.